J. Plasma Phys. (2025), *vol*. 91, E19
Published by Cambridge University Press

doi:10.1017/S0022377824001363

Multi-scale physics of magnetic reconnection in hot magnetized plasmas

Magali Muraglia[1],†, **Olivier Agullo**[1], **Nicolas Dubuit**[1], **Roméo Bigué**[1,2] and **Xavier Garbet**[2,3]

[1]Aix-Marseille Université, CNRS, PIIM UMR7345, Marseille, France

[2]CEA, IRFM, Saint-Paul-lez-Durance, F-13108 France

[3]School of Physical and Mathematical Sciences, NTU, 637371, Republic of Singapore

(Received 22 April 2024; revised 27 September 2024; accepted 1 October 2024)

Magnetic reconnection leads to the formation of island-shaped magnetic structure(s). Due to disagreement between theoretical evaluations of the characteristic reconnection time and observations, it is commonly accepted that the collisionality (or resistivity) is too low to explain magnetic reconnection phenomena in fusion plasmas. Thus, magnetic reconnection still raises many open questions. The work presented here aims to improve the fundamental knowledge about 'the life of a magnetic island'. Here, in the light of the many works of the last 70 years, a new paradigm for understanding magnetic reconnection in fusion plasmas is proposed. The life of a magnetic island (whatever its scale) follows three phases: the origin, the growth and the saturation. The possible physical mechanisms at play in these three phases will be investigated. First, for the island origin, typical time scales in link with magnetic reconnection will be evaluated for three tokamaks of different sizes (TCV, WEST and JET) to verify if magnetic reconnection is such an unexplained phenomenon in fusion plasmas. Second, for the island drive, the richness of possible mechanisms leading to 'rapid' magnetic island growth in fusion devices will be presented for small and large scales. Third comes the island saturation step. Results on the prediction of a large island width at saturation are presented and discussed.

Keywords: fusion plasma, plasma simulation, plasma nonlinear phenomena

1. Introduction

That magnetic field-line topology and its evolution are crucial for plasma dynamics, which has been known since the pioneering works of Alfvén (1950) and Dungey (1953). Ideally, the magnetic field and plasma are bound together. This is the well-known frozen-in law for a magnetic field immersed in a moving plasma: ideally, in a moving plasma flow, the magnetic flux and the magnetic connectivity are conserved in time. However, under non-ideal effects which break the frozen-in law, magnetic connectivity cannot be conserved: a magnetic field line can tear and then reconnect into a different topology. This

† Email address for correspondence: magali.muraglia@univ-amu.fr

fundamental process is described by an elegant physical concept: magnetic reconnection (Biskamp 2000).

Magnetic reconnection is ubiquitous in nature. It is observed in space plasmas: as an example, during solar flares, reconnection processes convert magnetic energy stored in a sunspot into kinetic energy accelerating locally particles (Giovanelli 1946). It is also observed in fusion plasma: non-ideal effects (like collisions/resistivity and/or electron inertia) initiate magnetic reconnection process where a global rearrangement of the magnetic field topology leads to the formation of magnetic island shape structure(s) characterized by their radial extension (also called island width). In the presence of an unstable current layer, leading to 'tearing-like' instabilities, the width of reconnected structure(s) (i.e. magnetic island(s)) grows in the linear phase and then is limited by nonlinear processes.

Magnetic reconnection is at the heart of various challenging open questions in fusion by magnetic confinement. Some of these questions are listed below.

(i) From a seed magnetic island (whose origin is still unknown) the nonlinear growth of radially large (a few tens of centimetres) magnetic island(s), called 'neoclassical tearing mode(s)' (NTMs) (Chang *et al.* 1995; La Haye 2006; Sauter *et al.* 2010), can destroy the equilibrium magnetic structure of a fusion plasma. Such modes lead to a brutal and catastrophic end of plasma discharge (i.e. disruption) and to a damage of the device walls. Advances have been made in recent years to control NTMs, which is essential for fusion plasmas (Kong *et al.* 2022). Improving such control strategies – these strategies are expensive and, some, time ineffective – requires improvement of understanding the physical mechanisms triggering NTMs (Muraglia *et al.* 2017; Kong *et al.* 2020).

(ii) The main scenario for operating most tokamaks, and the future device ITER, is based on an improved confinement regime where the turbulence intensity is reduced in a layer located at the plasma edge, called the 'pedestal'. Such improved regimes, known as the high-confinement mode (H-mode), experience edge localized modes (ELMs) that are busty edge perturbations. Having a predictive understanding of the physics of an ELM is still an open question (Snyder *et al.* 2002). Recent works (Hamed *et al.* 2019; Hatch *et al.* 2021; Hamed *et al.* 2023) have highlighted that the electron temperature gradient in the pedestal can drive microtearing modes creating small (of the order of millimetres) reconnected structures. The resulting electron heat transport, which is still not fully understood, is required to develop predictive pedestal models, which is of the utmost importance for the success of fusion by magnetic confinement.

(iii) Sawtooth crashes can, on the one hand, degrade the performance of fusion devices by driving NTMs while, on the other hand, preserve it by flushing impurities out of the core. The theoretical understanding of this phenomenon is still incomplete. In particular, the role of magnetic reconnection, which occurs during crashes, must be investigated in more detail (Samoylov *et al.* 2022; Yu & Günter 2022).

(iv) The observation of runaway electrons in post-disruption plasmas is another phenomenon where understanding the role of magnetic reconnection is critical. This is because the runaway current can replace the plasma current in its entirety and drives a reconnection event (Helander *et al.* 2007; Grasso *et al.* 2022) which affects the spread of the runaway-electrons beam when it hits the wall.

(v) In the so-called hybrid regime where the magnetic shear is low in the core region, an accumulation of high-charge impurities is often observed in the plasma core.

https://doi.org/10.1017/S0022377824001363 Published online by Cambridge University Press

Magnetic islands due to magnetohydrodynamics (MHD) processes are suspected to locally accelerate the penetration of impurities (Hender *et al.* 2016).

(vi) Recently, there has been renewed interest in the international community in magnetic configurations that are smaller than present-day machines, such as field-reversed configurations (FRCs) (Guo *et al.* 2015). These smaller machines require a high magnetic field, and magnetic reconnection will play a major role in their stability. The relevance for fusion applications of these FRCs has not yet been demonstrated, which adds to the importance of studies aimed at improving the understanding of the physical mechanisms related to magnetic reconnection.

In magnetic reconnection processes of plasmas fusion, various physical mechanisms can be at play, and the width of the resulting magnetic island(s) ranges from a millimetre (Hazeltine, Dobrott & Wang 1975; Drake & Lee 1977; Pueschel *et al.* 2013; Hamed *et al.* 2019), to a few tens of centimetres (Furth, Rutherford & Selberg 1973; Muraglia *et al.* 2011; Frank *et al.* 2020), i.e. a fraction of the radial extent of the plasma. The impact on confinement and transport depends on the width, the characteristic frequencies and the spatial distribution of the generated magnetic island(s). Although most fusion devices probably exhibit magnetic islands with a radial width continuum, various efforts over the last decades have separately focussed on the macro- and small-scales phenomena of magnetic reconnection. Indeed, the theoretical and numerical tools are quite different due to the scale differences involved. The MHD description (Agullo *et al.* 2014; Poyé *et al.* 2015; Agullo *et al.* 2017*a*,*b*; Muraglia *et al.* 2017) of large magnetic island dynamics has proven to be a successful framework for both the study of fundamental phenomena and predictions. At small scales, the microtearing instability requires a kinetic and/or a gyrokinetic description (Applegate *et al.* 2007; Doerk *et al.* 2011; Hatch *et al.* 2012; Dickinson *et al.* 2013; Predebon & Sattin 2013; Hatch *et al.* 2016; Hamed *et al.* 2018*a*,*b*, 2019, 2023; Hatch *et al.* 2021). Moreover, recently, strong efforts have been devoted to the investigation of the large-scale tearing mode using a gyrokinetic framework (Hornsby *et al.* 2015*b*, *a*, 2016; Bardóczi *et al.* 2017).

Magnetic reconnection is finally a multi-physics and multi-scale process. Nevertheless, there is no fundamental reason precluding a global vision of magnetic reconnection in fusion devices. Indeed, one can identify a ‘general magnetic island recipe’: whatever the scales and the physical ingredients involved, a magnetic reconnection process will always follow the same steps described by ‘the magnetic island life’. These steps are: (1) origin of magnetic island; (2) its growth; and finally (3) its saturation. These three steps are related to fundamental issues that should be addressed to enable solutions for critical fusion problems and provide a framework to investigate magnetic reconnection in fusion devices. Thus, in the light of many works of the last 70 years, a new paradigm for understanding and studying two-dimensional magnetic reconnection in fusion plasmas is proposed here following the framework of the magnetic island life. The paper is organized following the three island life steps.

First (§ 2), to have a magnetic island, a physical mechanism allowing the rearrangement of the magnetic field topology is required. Although several candidates exist (collisions/resistivity (Muraglia *et al.* 2011; Hornsby *et al.* 2015*a*; Hamed *et al.* 2019), electron inertia (Coppi *et al.* 1979; Grasso, Tassi & Waelbroeck 2010; Tassi *et al.* 2018; Grasso *et al.* 2020), electron anisotropy (Cassak *et al.* 2015; Granier *et al.* 2021), etc.), the identification of the dominant mechanisms leading to initial island-shaped structures is still an open problem and concerns an important fraction of the magnetic reconnection phenomena taking place in fusion devices. In this section, this question is investigated again following the new paradigm proposed here, i.e. by distinguishing the physical

https://doi.org/10.1017/S0022377824001363 Published online by Cambridge University Press

mechanism that initially breaks the frozen-in law to generate a magnetic island from the one that drives the growth of the island (this second step of the island life being investigated in § 3). In particular, typical time scales in link with magnetic reconnection will be computed for three tokamaks of different sizes (TCV, WEST and JET).

The second step of the island life concerns the growth of the magnetic island (§ 3). A physical mechanism (which is not necessarily the one which originates in the magnetic island) is required to drive the island growth. Once again, many candidates exist (magnetic equilibrium and collisions (Hornsby *et al.* 2015*a*), turbulent modes (Muraglia *et al.* 2011; Hornsby *et al.* 2015*b*, 2016; Poyé *et al.* 2015; Bardóczi *et al.* 2017; Ishizawa, Kishimoto & Nakamura 2019; Dubuit *et al.* 2021), electric temperature gradient (Applegate *et al.* 2007; Doerk *et al.* 2011; Dickinson *et al.* 2013; Predebon & Sattin 2013; Hamed *et al.* 2019; Hatch *et al.* 2021; Hamed *et al.* 2023), bootstrap current (Sauter *et al.* 2010; Kong *et al.* 2020, 2022), Hall effect, electron anisotropy (Cassak *et al.* 2015; Granier *et al.* 2021), etc.). The question of the drive is still open at the small scale (for microtearing modes) as well at the large scale (origin of the seed island required for the nonlinear growth of a NTM as an example). Here, a review of possible mechanisms leading to a magnetic island growth (at small scale as well as at large scale) and their relevance for the fusion context is presented.

Third comes the last step of saturation (§ 4). Once again, saturation mechanisms are still unknown at the small scale as well as at the large scale. Here, the focus will only be on the possible saturation mechanisms for predicting the saturated island width in a case of a large magnetic island (saturation at small scale for microtearing modes remaining a fully open question). Since the pioneer work of Rutherford (Rutherford 1973) where a first model has been derived to predict the saturated island width, many works have subsequently been performed to improve this first model (Carrera, Hazeltine & Kotschenreuther 1986; Escande & Ottaviani 2004; Militello & Porcelli 2004; Smolyakov *et al.* 2013) and to test their validity against simulations. Here, a review of these past studies is presented showing that although generalized Rutherford models are widely and successfully used in experiment (Sauter *et al.* 2010; Kong *et al.* 2020, 2022), their agreement with first principle numerical simulations still needs to be demonstrated (Militello, Grasso & Borgogno 2014; Poyé *et al.* 2014; Muraglia *et al.* 2021).

In the last part dedicated to the conclusions (§ 5), a summary and open questions related to magnetic reconnection in fusion plasmas will be drawn.

2. Origin

2.1. *What is magnetic reconnection?*

Magnetic reconnection is a concept that primarily relates to electromagnetic phenomena taking place in a medium in the plasma state. Naturally, the theoretical framework of magnetic reconnection is initially linked to the motion of a plasma immersed in a magnetic field and is, as a consequence, intimately linked to the concept of field-line motion, which was first introduced by H. Alfvén in 1945 (Alfvén 1950) and was developed later by J. W. Dungey in 1953 (Dungey 1953). Starting with the historical point of view (i.e. using a fluid approach), one can consider a bath of charged, moving and non-relativistic particles immersed in an electromagnetic field ($\boldsymbol{E}, \boldsymbol{B}$). At large scales, the charge distribution is such that the plasma is electrically neutral and the fluid framework is usually adopted to describe the plasma behaviour. Due to the coupling of the plasma with the electromagnetic field ($\boldsymbol{E}, \boldsymbol{B}$), a complete description of the dynamics requires a coupling of the fluid equations to the Maxwell equations: this framework is well known as the MHD model that offers an efficient understanding of the magnetic reconnection concept (Biskamp 2000). As a starting point to understand magnetic reconnection, one can investigate the impact

https://doi.org/10.1017/S0022377824001363 Published online by Cambridge University Press

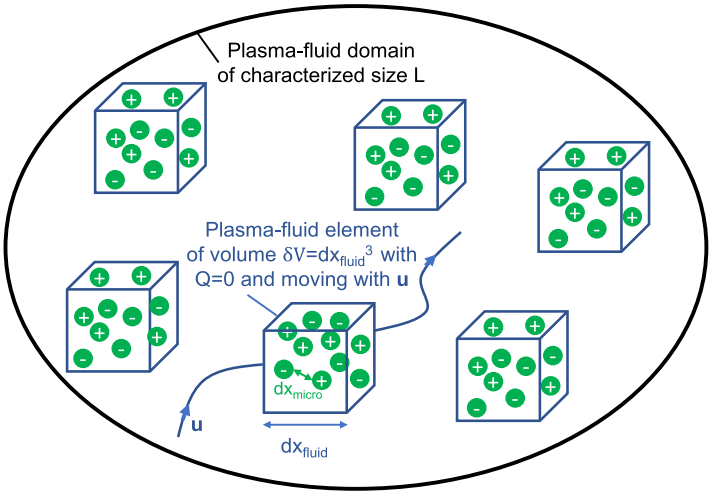

FIGURE 1. Notion of plasma-fluid element: plasma is a multi-scale medium where $L \gg \mathrm{d}x_{\mathrm{fluid}} \gg \lambda_D \gg \mathrm{d}x_{\mathrm{micro}}$ (λ_D is the Debye length). There exist three main levels of description that can be used to model plasma dynamics: particulate at scale $\mathrm{d}x_{\mathrm{micro}}$, kinetic at scale $\mathrm{d}x_{\mathrm{micro}}$, fluid at a larger scale $\mathrm{d}x_{\mathrm{fluid}}$. For a plasma-fluid element, quasi-neutrality is conserved (i.e. $Q = 0$) since $\mathrm{d}x_{\mathrm{fluid}} \gg \lambda_D$. The fluid velocity $\boldsymbol{u}$ can be evaluated from the MHD framework.

of a plasma-fluid element (figure 1) moving with $\boldsymbol{u}$ through a magnetic field $\boldsymbol{B}$ on this magnetic field in terms of magnetic flux and magnetic connectivity.

2.1.1. *Magnetic flux balance*

One can consider two times t_1 and t_2 during which the plasma-fluid element displacement is $\boldsymbol{u}(t_2 - t_1) = \boldsymbol{u}\Delta t$ (figure 2). At time t_1, the magnetic flux Φ_1 through the surface S_1 bounded by the contour C_1 is

$$\Phi_1 = \int_{S_1} \boldsymbol{B}\,(\boldsymbol{x}, t) \cdot \boldsymbol{dS_1}, \tag{2.1}$$

where $\boldsymbol{d}_{S_1}$ is the oriented surface element related to the surface S_1.

At time $t_2 = t + \Delta t$, the plasma-fluid element has moved by a distance $\boldsymbol{u}\Delta t$ and crosses a new surface S_2 (deformed with respect to S_1) and delimited by the contour C_2 (also deformed with respect to C_1). The magnetic flux Φ_2 through this new surface is $\Phi_2 = \int_{S_2} \boldsymbol{B}(\boldsymbol{x}, t) \cdot \boldsymbol{dS_2}$ (with $\boldsymbol{dS_2}$ being the oriented surface element related to S_2).

A first Taylor expansion, in time, gives $\Phi_2 \sim \int_{S_2} \boldsymbol{B}(\boldsymbol{x} + \boldsymbol{u}\Delta t, t) \cdot \boldsymbol{dS_2} + \Delta t \int_{S_2} \partial_t \boldsymbol{B}(\boldsymbol{x} + \boldsymbol{u}\Delta t, t) \cdot \boldsymbol{dS_2}$. Then, a second Taylor expansion in $\boldsymbol{x}$ (with $\boldsymbol{dx} = \boldsymbol{u}\Delta t$) gives $\boldsymbol{B}(\boldsymbol{x} + \boldsymbol{u}\Delta t, t) \sim \boldsymbol{B}(\boldsymbol{x}, t) + \boldsymbol{u}\Delta t(\partial \boldsymbol{B}(\boldsymbol{x}, t)/\partial \boldsymbol{x})$, where the position $\boldsymbol{x}$ is related to the surface S_1 and the position $\boldsymbol{x} + \boldsymbol{u}\Delta t$ is related to the surface S_2. Finally, keeping only the order 1 terms (with $\Delta t \ll \Delta t^2$), the linearized Φ_2 can be written as

$$\Phi_2 \sim \int_{S_2} \boldsymbol{B}\,(\boldsymbol{x} + \boldsymbol{u}\Delta t, t) \cdot \boldsymbol{dS_2} + \Delta t \int_{S_1} \partial_t \boldsymbol{B}\,(\boldsymbol{x}, t) \cdot \boldsymbol{dS_1}. \tag{2.2}$$

Applying the Ostrogradski theorem to the local Maxwell–Thomson equation, it is well known that at a given time, $\int_V \boldsymbol{\nabla} \cdot \boldsymbol{B}\,\mathrm{d}V = \int_S \boldsymbol{B} \cdot \boldsymbol{dS} = 0$, where $S = S_1 + S_2 + S_L$ (with $\boldsymbol{dS}$ its associated oriented surface element) is the surface enveloping the volume

https://doi.org/10.1017/S0022377824001363 Published online by Cambridge University Press

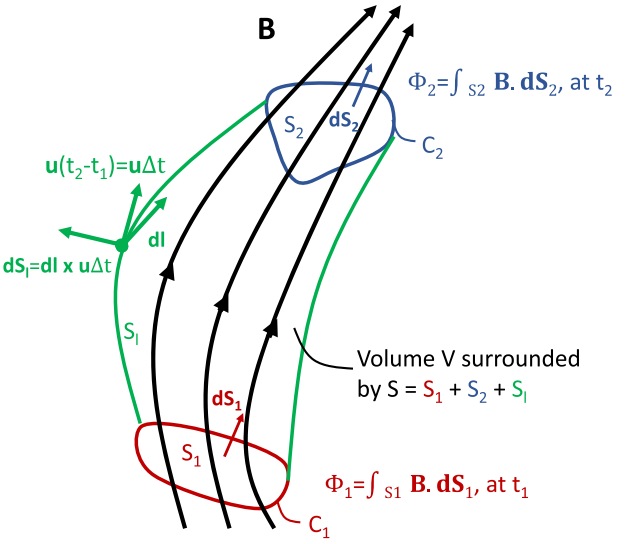

FIGURE 2. Magnetic flux balance.

V crossed by the plasma-fluid element. At a time t, the plasma-fluid element 'enters' by S_1 and 'leaves' the volume V through S_2 and S_l. This simple balance of flows gives

$$\int_S \boldsymbol{B}\cdot\boldsymbol{dS}=0=-\int_{S_1}\boldsymbol{B}(\boldsymbol{x},t)\cdot\boldsymbol{dS_1}+\int_{S_2}\boldsymbol{B}(\boldsymbol{x}+\boldsymbol{u}\Delta t,t)\cdot\boldsymbol{dS_2}+\int_{S_l}\boldsymbol{B}(\boldsymbol{x},t)\cdot\boldsymbol{dS_l}. \tag{2.3}$$

Using the expressions of the fluxes Φ_1 (2.1) and Φ_2 (2.2), one can write

$$\Phi_1-\Phi_2+\Delta t\int_{S_1}\partial_t\boldsymbol{B}(\boldsymbol{x},t)\cdot\boldsymbol{dS_1}-\int_{S_l}\boldsymbol{B}(\boldsymbol{x},t)\cdot\boldsymbol{dS_l}=0. \tag{2.4}$$

Then (figure 2), on the lateral surface S_l, $\boldsymbol{dS_l}=\boldsymbol{dl}\times\boldsymbol{u}\Delta t$, where $\boldsymbol{dl}$ is the oriented displacement element along the contour $C_l=C_1$ which is the common boundary of the surfaces S_1 and S_l. Using the Stokes theorem, one can get $\int_{S_l}\boldsymbol{B}\cdot\boldsymbol{dS_l}=\int_{C_l}\boldsymbol{B}\cdot(\boldsymbol{dl}\times\boldsymbol{u}\Delta t)=\Delta t\int(\boldsymbol{u}\times\boldsymbol{B})\cdot\boldsymbol{dl}=\Delta t\int_{S_1}\nabla\times(\boldsymbol{u}\times\boldsymbol{B})\cdot\boldsymbol{dS_1}$.

Finally, the flux balance (2.4) can be re-written using the Maxwell–Faraday equation and representing the conservation (or the non-conservation) of the magnetic flux during the plasma motion:

$$\frac{\mathrm{d}\Phi}{\mathrm{d}t}=\frac{\Phi_2-\Phi_1}{\Delta t}=\int_{S_1}[-\nabla\times(\boldsymbol{E}+\boldsymbol{u}\times\boldsymbol{B})]\cdot\boldsymbol{dS_1}. \tag{2.5}$$

2.1.2. *Magnetic connectivity*

At a given time t, M_1 is a plasma-fluid element of the magnetic field line moving with $\boldsymbol{u_1}\equiv\boldsymbol{u}$ and M_2 is another plasma-fluid element (moving with $\boldsymbol{v_2}$) belonging to the same line and very close to M_1: M_1 and M_2 are separated by the infinitesimal length $\boldsymbol{\Delta l}$ and $\Delta\boldsymbol{u}=\boldsymbol{u_2}-\boldsymbol{u}$ (figure 3). By definition, magnetic field lines are parallel at any point of the magnetic field $\boldsymbol{B}$ leading to $\boldsymbol{\Delta l}\times\boldsymbol{B}=\boldsymbol{0}$, and it is said that M_1 and M_2 are connected by the same magnetic field line. The notion of magnetic reconnection is therefore naturally linked to the non-conservation (between two moments t and $t+dt$) of

https://doi.org/10.1017/S0022377824001363 Published online by Cambridge University Press

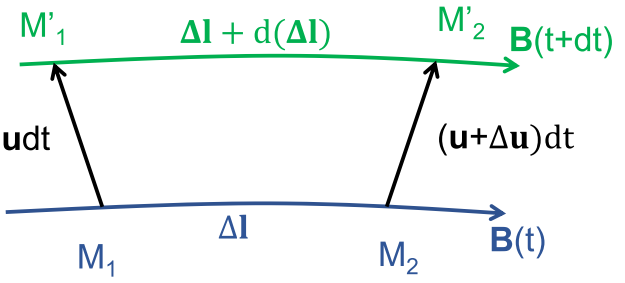

FIGURE 3. Magnetic connectivity concept. At t, M_1 and M_2 belong to the same magnetic field line: they are connected and $\boldsymbol{\Delta l} \times \boldsymbol{B} = \boldsymbol{0}$. If the connectivity is conserved, at $t + dt$, M_1' and M_2' still belong to the same magnetic field line and $(\boldsymbol{\Delta l} + d(\boldsymbol{\Delta l})) \times \boldsymbol{B} = \boldsymbol{0}$.

this magnetic connectivity which should be investigated by computing $(\mathrm{d}/\mathrm{d}t)(\boldsymbol{\Delta l} \times \boldsymbol{B}) = \underbrace{(\mathrm{d}\boldsymbol{\Delta l}/\mathrm{d}t) \times \boldsymbol{B}}_{I} + \underbrace{\boldsymbol{\Delta l} \times \mathrm{d}\boldsymbol{B}/\mathrm{d}t}_{II}$.

To that purpose, figure 3 is plotted: M_1' and M_2' are respectively M_1 and M_2 after dt. An evaluation of I[1] gives $\mathrm{d}\boldsymbol{\Delta l}/\mathrm{d}t \times \boldsymbol{B} = [(\boldsymbol{B} \cdot \boldsymbol{\nabla})\boldsymbol{u}] \times \boldsymbol{\Delta l}$. Additionally, an evaluation of II[2] gives $\boldsymbol{\Delta l} \times \mathrm{d}\boldsymbol{B}/\mathrm{d}t = [\boldsymbol{\nabla} \times \boldsymbol{E} - (\boldsymbol{u} \cdot \boldsymbol{\nabla})\boldsymbol{B}] \times \boldsymbol{\Delta l}$. As a consequence, one can write that $(\mathrm{d}/\mathrm{d}t)(\boldsymbol{\Delta l} \times \boldsymbol{B}) = I + II = [(\boldsymbol{B} \cdot \boldsymbol{\nabla})\boldsymbol{u} + \boldsymbol{\nabla} \times \boldsymbol{E} - (\boldsymbol{u} \cdot \boldsymbol{\nabla})\boldsymbol{B}] \times \boldsymbol{\Delta l}$. Finally, thanks to vector identities, one can write the conservation (or the non-conservation) of the magnetic connectivity:

$$\frac{\mathrm{d}}{\mathrm{d}t}(\boldsymbol{\Delta l} \times \boldsymbol{B}) = [\boldsymbol{\nabla} \times (\boldsymbol{E} + \boldsymbol{u} \times \boldsymbol{B})] \times \boldsymbol{\Delta l}. \tag{2.6}$$

2.1.3. *Frozen-in law and general definition of magnetic reconnection*

It is very interesting to highlight that, so far, the fluid character of the plasma has not been used, in particular, to obtain (2.5) and (2.6). M_1 and M_2 have been considered as a plasma-fluid volume element $\delta V = \mathrm{d}x^3_{\mathrm{fluid}}$ (see figure 1) attached to the magnetic field line as well as to a single point that belongs to this line. However, at this stage, it is useful to use the MHD framework where M_1 and M_2 are plasma-fluid volume elements moving with the fluid velocity $\boldsymbol{u}$ which satisfies the well-known generalized Ohm's law (Biskamp 2000):

$$\boldsymbol{E} = \boldsymbol{E}_{ind} + \boldsymbol{E}_{Ohm} + \boldsymbol{E}_{Hall} + \boldsymbol{E}_{iner} + \boldsymbol{E}_{therm}. \tag{2.7}$$

In (2.7):

(i) $\boldsymbol{E}_{ind} = -\boldsymbol{u} \times \boldsymbol{B}$ is the ideal induction or dynamo field representing the electric field created by the global motion $\boldsymbol{u}$ of the plasma within the magnetic field $\boldsymbol{B}$. It plays at large fluid scale L (see figure 1);

(ii) $\boldsymbol{E}_{Ohm} = \eta \boldsymbol{j}$ is the non-ideal ohmic field, the plasma being an electric conductor of resistivity η and of current $\boldsymbol{j}$. This term becomes important in thin resistive layer $L_\eta \ll L$ (see further for an evaluation of L_η for typical tokamaks);

[1]From figure 3, one can write that $\cancel{\boldsymbol{\Delta l}} + (\cancel{\boldsymbol{u}} + \boldsymbol{\Delta u})\,\mathrm{d}t = \cancel{\boldsymbol{u}}\,\mathrm{d}t + \cancel{\boldsymbol{\Delta l}} + \mathrm{d}(\boldsymbol{\Delta l})$ giving $\boldsymbol{\Delta u} = \boldsymbol{u_2} - \boldsymbol{u} = \mathrm{d}(\boldsymbol{\Delta l})/\mathrm{d}t$. A first-order Taylor expansion of $\boldsymbol{u}$ along the magnetic field line leads to $\boldsymbol{u_2} = \boldsymbol{u} + (\boldsymbol{\Delta l} \cdot \boldsymbol{\nabla})\boldsymbol{u}$ and then $\mathrm{d}(\boldsymbol{\Delta l})/\mathrm{d}t = (\boldsymbol{\Delta l} \cdot \boldsymbol{\nabla})\boldsymbol{u}$. Moreover, $\boldsymbol{B} = |\boldsymbol{B}|\boldsymbol{b}$ and as $\boldsymbol{\Delta l} \times \boldsymbol{B} = \boldsymbol{0}$, one can write $\boldsymbol{\Delta l} = |\boldsymbol{\Delta l}|\boldsymbol{b}$. As a consequence, $\mathrm{d}\boldsymbol{\Delta l}/\mathrm{d}t \times \boldsymbol{B} = [|\boldsymbol{\Delta l}||\boldsymbol{B}|(\boldsymbol{b} \cdot \boldsymbol{\nabla})\boldsymbol{u}] \times \boldsymbol{b} = [(\boldsymbol{B} \cdot \boldsymbol{\nabla})\boldsymbol{u}] \times \boldsymbol{\Delta l}$.

[2]Separating the local variation of $\boldsymbol{B}$ and its advection by $\boldsymbol{u}$, one can write the particular derivative $\mathrm{d}\boldsymbol{B}/\mathrm{d}t = \partial_t \boldsymbol{B} + (\boldsymbol{u} \cdot \boldsymbol{\nabla})\boldsymbol{B}$. Additionally, using the Maxwell–Faraday equation, II is evaluated as $\boldsymbol{\Delta l} \times \mathrm{d}\boldsymbol{B}/\mathrm{d}t = [\boldsymbol{\nabla} \times \boldsymbol{E} - (\boldsymbol{u} \cdot \boldsymbol{\nabla})\boldsymbol{B}] \times \boldsymbol{\Delta l}$.

https://doi.org/10.1017/S0022377824001363 Published online by Cambridge University Press

(iii) $\boldsymbol{E_{Hall}} = (1/n_e e)\boldsymbol{j} \times \boldsymbol{B}$ is the non-ideal Hall field corresponding to the Lorentz force $\boldsymbol{j} \times \boldsymbol{B}$ (n_e being the fluid density of the electrons and e being the elementary charge). This term becomes important at scales of the order of the ionic Larmor radius $\rho_i \ll L_\eta \ll L$;

(iv) $\boldsymbol{E_{iner}} = (m_e/n_e e^2)[\partial_t \boldsymbol{j} + \boldsymbol{\nabla} \cdot (\overline{\overline{\boldsymbol{uj}}} + \overline{\overline{\boldsymbol{ju}}} - (1/n_e e)\overline{\overline{\boldsymbol{jj}}})]$ (where $\bar{\bar{\bullet}}$ represents a tensor) is the non-ideal inertial term which plays a role at scales of the order of the electron skin depth $d_e \ll \rho_i \ll L_\eta \ll L$ (m_e being the electron mass);

(v) $\boldsymbol{E_{therm}} = -(1/n_e e)\boldsymbol{\nabla} \cdot \overline{\overline{P_e}}$ is the non-ideal thermal electromotive field playing a role at ion sound Larmor radius scale being smaller than L and with $\overline{\overline{\boldsymbol{P_e}}}$ being the electron's pressure tensor.

Thus, at large scale, non-ideal effects can be neglected and the ideal Ohm's law is simply $\boldsymbol{E} = \boldsymbol{E_{ind}} = -\boldsymbol{u} \times \boldsymbol{B}$ leading to a conservation of the magnetic flux ((2.5) becomes $\mathrm{d}\Phi/\mathrm{d}t = 0$) and the magnetic connectivity ((2.6) becomes $(\mathrm{d}/\mathrm{d}t)(\boldsymbol{\Delta l} \times \boldsymbol{B}) = 0$). This is the well-known frozen-in law, where at large scale, the plasma and the magnetic field $\boldsymbol{B}$ are strongly coupled in the same dynamic and where magnetic reconnection cannot occur.

However at smaller scales, non-ideal effects can originate from an electric field leading to a non-conservation of the magnetic connectivity with (2.6) becoming

$$\frac{\mathrm{d}}{\mathrm{d}t}(\boldsymbol{\Delta l} \times \boldsymbol{B}) = \left[\boldsymbol{\nabla} \times \boldsymbol{E}^{NI}\right] \times \boldsymbol{\Delta l} \neq 0. \tag{2.8}$$

To go further by investigating the required form of $\boldsymbol{E}^{NI}$ leading to a non-conservation of magnetic connectivity (2.8), a general definition of magnetic reconnection can be drawn. Indeed, magnetic reconnection is due to a particular dynamics of the magnetic field and as a consequence of the Faraday law due to the existence of non-zero rotational electric field. However, not all rotational electric fields can lead to magnetic reconnection. More precisely, having $\boldsymbol{E}^{NI} \neq \boldsymbol{0}$ is not sufficient to allow magnetic reconnection. Additionally, to get a general definition of magnetic reconnection, the impact of the form of $\boldsymbol{E}^{NI}$ has to be investigated on (2.5) and (2.8). Let us set $\boldsymbol{E}^{NI} = \boldsymbol{E}^{NI}_{\parallel} + \boldsymbol{E}^{NI}_{\perp}$, where the subscripts $_\parallel$ and $_\perp$ refer respectively to the parallel direction to $\boldsymbol{B} = B\boldsymbol{b}$ with $\boldsymbol{E}^{NI}_{\parallel} = (\boldsymbol{b} \cdot \boldsymbol{E}^{NI})\boldsymbol{b}$ and to the orthogonal direction with $\boldsymbol{E}^{NI}_{\perp} = \boldsymbol{b} \times (\boldsymbol{E}^{NI} \times \boldsymbol{b})$. Thus, $\boldsymbol{E}^{NI}_{\perp}$ can be written as $\boldsymbol{E}^{NI}_{\perp} = \boldsymbol{v} \times \boldsymbol{B}$, where the physical meaning of the velocity $\boldsymbol{v}$ will be understood just after. As a consequence, $\boldsymbol{E}^{NI} = \boldsymbol{E}^{NI}_{\parallel} + \boldsymbol{v} \times \boldsymbol{B}$. The expression of the generalized Ohm's law written as $\boldsymbol{E} = -\boldsymbol{u} \times \boldsymbol{B} + \boldsymbol{v} \times \boldsymbol{B} + \boldsymbol{E}^{NI}_{\parallel}$ leads to the following expression for the conservation of the magnetic flux (2.5):

$$\frac{\mathrm{d}\Phi}{\mathrm{d}t} = \int_{S_1} -\left[\boldsymbol{\nabla} \times \boldsymbol{E}^{NI}{}_{\parallel}\right] \cdot \boldsymbol{dS}_1 \tag{2.9}$$

and for the conservation of the magnetic connectivity (2.8):

$$\frac{\mathrm{d}}{\mathrm{d}t}(\boldsymbol{\Delta l} \times \boldsymbol{B}) = \left[\boldsymbol{\nabla} \times \boldsymbol{E}^{NI}_{\parallel}\right] \times \boldsymbol{\Delta l} \tag{2.10}$$

in the moving frame of velocity $\boldsymbol{w} = \boldsymbol{u} - \boldsymbol{v}$ with $\mathrm{d}/\mathrm{d}t = \partial_t + \boldsymbol{w} \cdot \boldsymbol{\nabla}$. One can note that the perpendicular non-ideal electric field $\boldsymbol{E}^{NI}_{\perp}$ does not contribute to the magnetic field connectivity conservation (2.10). From (2.9) and (2.10), one can conclude that the perpendicular component of the non-ideal terms in generalized Ohm's law (2.7) written as $\boldsymbol{E}^{NI}_{\perp} = \boldsymbol{v} \times \boldsymbol{B}$ leads only to a non-conservation of the magnetic flux (2.9) in the plasma flow frame of velocity $\boldsymbol{u}$.

https://doi.org/10.1017/S0022377824001363 Published online by Cambridge University Press

So having $\boldsymbol{E}^{NI} = \boldsymbol{E}^{NI}_{\perp}$ in a thin non-ideal layer does not originate in magnetic reconnection. However, this term leads to a slippage of the magnetic field line moving at a velocity $\boldsymbol{v}$ different to the plasma velocity $\boldsymbol{u}$. (It is interesting to note that in the generalized Ohm's law (2.7), the Hall term $\boldsymbol{E}_{\boldsymbol{Hall}}$ induces such slippage of magnetic field lines and can accelerate (without originating it) magnetic reconnection.) Finally, following (2.9) and (2.10), only the parallel component of the non-ideal electric field $\boldsymbol{E}^{NI}_{\parallel}$ in the generalized Ohm's law (2.7) leads to a non-conservation of magnetic connectivity in a thin non-ideal layer and as a consequence leads to magnetic reconnection.

In the past (Vasyliunas 1975; Axford 1984; Sonnerup 1984; Schindler & Hesse 1988; Hornig & Rastätter 1997, 1998; Priest & Forbes 1998), from a general form of $\boldsymbol{E}^{NI}$, attempts have been made to provide a general definition of magnetic reconnection and some questions are still open today. Here, associating the magnetic reconnection to a non-conservation of magnetic connectivity given by (2.10) and following the point of view of Schindler & Hesse (1988), a general definition of magnetic reconnection is given: having $\boldsymbol{E}^{N}_{\parallel} \neq \boldsymbol{0}$ in a extremely thin region is a necessary and sufficient condition for general magnetic reconnection in two-dimensional (2-D) as well as in three-dimensional (3-D) space. Magnetic reconnection is the result of a local non-conservation of magnetic connectivity between two times due to non-ideal effects leading to the presence of $\boldsymbol{E}^{NI}_{\parallel}$ in the thin non-ideal region. The 2-D process can be illustrated by figure 4 where magnetic field lines are not conserved during the magnetic reconnection process: two plasma-fluid elements P_1, P_2 (regardless of the distance separating them), connected by the same magnetic field line at a given time, are no longer so after the magnetic field lines have been disconnected and then reconnected. Thus, magnetic reconnection is by nature a multi-scale process. Most of the time, the frozen-in law is satisfied, the plasma and the magnetic field being strongly attached together. However, there exist extremely thin regions where non-ideal effects become important to break the frozen-in law. In these non-ideal regions (also known as diffusive regions), magnetic field lines can experience a local tearing and then a local reconnection leading to a global change of magnetic field topology and to the formation of magnetic island(s) (for a 2-D picture, see figure 4). It is said that the magnetic field diffuses through the plasma. As mentioned in the introduction, although the historical point of view emphasizes large-scale topology changes, the resulting structures (with an island shape) can develop on both small and large scales.

2.2. *Inventory of possible mechanisms at the origin of magnetic reconnection in fusion plasmas*

In the MHD framework, the possible mechanisms leading to magnetic reconnection are summarized in the generalized Ohm's law (2.7) where the $\boldsymbol{E}_{\boldsymbol{Ohm}}$, $\boldsymbol{E}_{\boldsymbol{iner}}$ and $\boldsymbol{E}_{\boldsymbol{therm}}$ terms exhibit the parallel component. Magnetic reconnection is well observed in fusion plasma meaning that one or more of these mechanisms should be at play. However, in the literature (Parker 1957; Sweet 1958*a*,*b*), from (2.7), evaluations of characteristic reconnection time τ_{RM} have been compared with observations in fusion plasma and disagreements have been found. Indeed, in these evaluations based on the so-called Sweet–Parker model, the characteristic reconnection time is derived from the mechanism driving the magnetic reconnection (magnetic island in 2-D) growth, the mechanism at the origin of the reconnection (the mechanism that breaks the frozen-in law) being not distinguished from the growing one. Thus, it has been found that in fusion plasma, due to the high core temperature, the resistivity is too weak to explain the growth of reconnected structures. In the same way, although the growth of magnetic islands due to electronic inertia is faster, it is commonly accepted that electronic inertia cannot explain the origin of the magnetic island in a fusion machine (due to the narrowness of the non-ideal layer generated by

https://doi.org/10.1017/S0022377824001363 Published online by Cambridge University Press

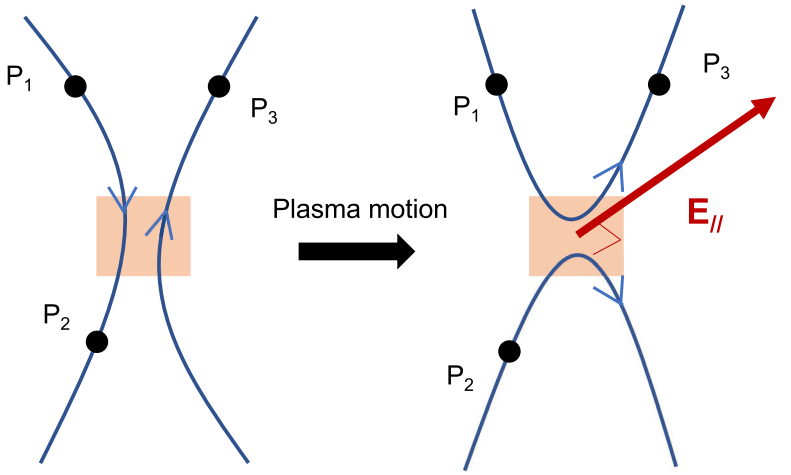

FIGURE 4. Simple picture of 2-D magnetic reconnection process. Before magnetic reconnection, P_1 and P_2 are connected by the same magnetic field line. The plasma-fluid element P_3 belongs to another magnetic field line. During the reconnection process, a narrow non-ideal region (in orange) forms between the oppositely directed field lines: magnetic reconnection is a non-ideal local process. After the reconnection, P_2 is no longer connected to P_1, but is now connected to P_3.

the electronic skin depth). Finally, the thermal electromotive field generates reconnected structures of the order of ρ_i being too small to be relevant in the fusion context. As a consequence, it is commonly accepted and stated that the origin of magnetic reconnection is still unknown in a fusion device.

However, there is no fundamental reason that the non-ideal mechanism at the origin of the reconnection (i.e. the mechanism which breaks the frozen-in law) is also the one that allows the island to grow. Thus, here, starting from the general magnetic reconnection definition, it is proposed to investigate the relevance in a fusion context of physical mechanisms breaking the frozen-in law without considering the growth of the generated magnetic island. In particular, typical time scales in line with magnetic reconnection will be computed for three tokamaks of different sizes (TCV, WEST and JET) to check if magnetic reconnection is indeed an unexplained phenomenon in fusion plasma.

2.2.1. *Sweet–Parker model*

Sweet and Parker were the first to propose a physical mechanism of magnetic reconnection (Parker 1957; Sweet 1958*a*,*b*). The so-called Sweet–Parker mechanism is a 2-D model of steady-state magnetic reconnection of a resistive current sheet in a plasma flow of velocity $\boldsymbol{u}$. To illustrate this model, let us consider a simple magnetic configuration in a 3-D slab geometry such as $\boldsymbol{B} = B_z\boldsymbol{e}_z + B_y x\boldsymbol{e}_y$ with $B_z \gg B_y$. Here, $B_z\boldsymbol{e}_z$ is called the guide field, where $\boldsymbol{e}_z$ is the parallel direction, and the reconnection process takes place in the 2-D perpendicular plane (x, y). For such configuration, in (x, y), along the line $x = 0$, the magnetic field is null and is of opposite sign on either side of the null points line. Resistivity is supposed to play a role only in a thin layer called the resistive or the diffusive layer of length $2L$ and width $2l$ and follows the null points line. In this layer, following the well-known Ampère law, the parallel current $\boldsymbol{j} = \mu_0^{-1}B_y\boldsymbol{e}_z$ induces a non-zero $\boldsymbol{E}_{\parallel}^{NI} = \eta\boldsymbol{j}$ (where μ_0 is the magnetic constant) leading to magnetic reconnection. From the generalized Ohm's law (2.7) in the resistive layer, $\boldsymbol{E} \sim \eta\boldsymbol{j}$, combined with the

https://doi.org/10.1017/S0022377824001363 Published online by Cambridge University Press

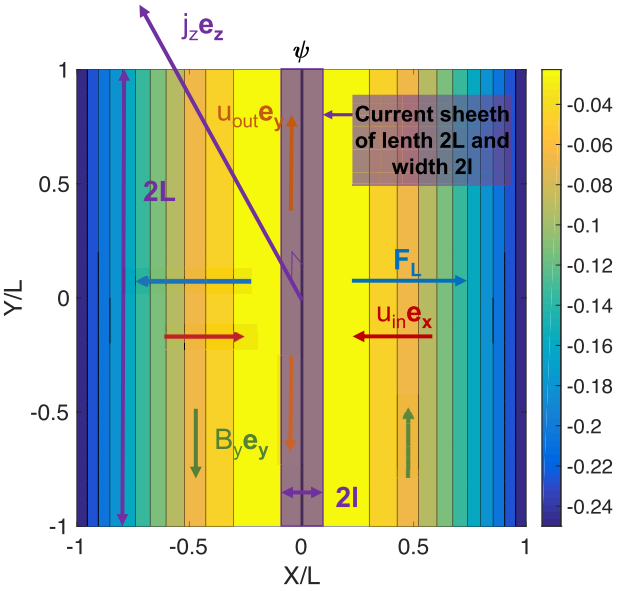

FIGURE 5. Illustration of the Sweet–Parker mechanism.

Faraday law, one can write the induction equation for the magnetic field: $\partial_t \boldsymbol{B} \sim \eta \boldsymbol{\Delta B}$. It is said that the magnetic field diffuses in the resistive layer. Outside the resistive layer, the system is considered as ideal where the coupling between the generalized Ohm's law (2.7), $\boldsymbol{E} \sim -\boldsymbol{u} \times \boldsymbol{B}$, and the well-known Faraday law gives the ideal induction equation for the magnetic field, $\partial_t B \sim \boldsymbol{\nabla} \times (\boldsymbol{u} \times \boldsymbol{B})$. In the (x, y) plane, the two components of the plasma flow $\boldsymbol{u}$ does not play the same role regarding the reconnection phenomena. The component along the x direction, i.e. $\boldsymbol{u_x} = \boldsymbol{u_{in}}$, 'pushes' the flow inside the resistive layer where magnetic reconnection can take place by the resistive diffusion of the magnetic field. Thus, it is assumed that $\boldsymbol{u_{in}}$ is directed along increasing x when $x < 0$ and along decreasing x when $x > 0$. The component along the y direction, i.e. $\boldsymbol{u_y} = \boldsymbol{u_{out}}$, is attached to the magnetic field and drives the flow outside the resistive layer. An illustration of the Sweet–Parker configuration is presented in figure 5.

First, the Sweet–Parker model proposes an elegant description of the physical mechanism at play at the resistive layer during a steady-state (i.e. ∂_t going to 0) magnetic reconnection process. As mentioned previously, the flow pushes the plasma inside the resistive layer. The counter-reaction to this flow pushing the magnetic field induces the existence of a Lorentz force opposing $\boldsymbol{u_{in}}$. In the MHD framework, the Lorentz force can be evaluated as $\boldsymbol{F_L} \sim \boldsymbol{j} \times \boldsymbol{B}$, where the current can be estimate taking the generalized Ohm's law (2.7) with only the inductive and resistive terms, i.e. $\boldsymbol{j} \sim (\boldsymbol{u} \times \boldsymbol{B})/\eta = (u_{in} B_y/\eta)\boldsymbol{e_z}$. It follows an estimation of the Lorentz force $\boldsymbol{F_L} \sim -(u_{in} B_y^2/\eta)\boldsymbol{e_x}$. Thus, in the ideal region where $u_{in} B_y^2 \neq 0$ and where $\eta \to 0$, magnetic reconnection is not allowed: the Lorentz force is infinite and prevents flow from breaking magnetic field lines that can only be distorted. However, in the resistive layer, $B_y(x = 0) = 0$ and since η is very small indeed, but has a finite value, one can write that $\boldsymbol{F_L} = 0$. There is no more counter-reaction to the incoming flow $\boldsymbol{u_{in}}$. The pressure applied by the incoming flow $\boldsymbol{u_{in}}$ on the magnetic field lines leads to the breaking of these field lines: magnetic reconnection occurs.

Then, the Sweet–Parker model gives an estimate of the magnetic reconnection time defined by Sweet and Parker as $\tau_{RM} = L/u_{in}$. To evaluate τ_{RM}, u_{in} has to be expressed as a

https://doi.org/10.1017/S0022377824001363 Published online by Cambridge University Press

TCV	$L \sim 0.25$ m, $B = 1.43$ T, $\eta \sim 10^{-5}\,\Omega\,\mathrm{cm}^1$	$\sqrt{\tau_\eta \tau_A} \sim 2$ h	$\sqrt{\tau_\eta^l \tau_A} \sim 10$ s
WEST	$L \sim 0.25$ m, $B = 3.7$ T, $\eta \sim 10^{-6}\,\Omega\,\mathrm{cm}^1$	$\sqrt{\tau_\eta \tau_A} \sim 3$ days	$\sqrt{\tau_\eta^l \tau_A} \sim 2$ min
JET	$L \sim 1$ m, $B = 3.45$ T, $\eta \sim 10^{-7}\,\Omega\,\mathrm{cm}^1$	$\sqrt{\tau_\eta \tau_A} \sim 115$ days	$\sqrt{\tau_\eta^l \tau_A} \sim 16$ min

TABLE 1. Estimation of the resistive characteristic reconnection time in the centre of TCV, WEST and JET using $\tau_{MR} \sim \sqrt{\tau_\eta \tau_A}$ (column 3) and using $\tau_{MR} \sim \sqrt{\tau_\eta^l \tau_A}$ (column 4).

function of the system parameters. To this end, one can start by using the incompressibility property of the flow (i.e. $\boldsymbol{\nabla} \cdot \boldsymbol{u} = 0$) to write that $u_{in}/l \sim u_{out}/L$. This leads to $u_{in} \sim (l/L)u_{out}$. For the steady-state regime, the induction equation in the resistive layer (i.e. considering the magnetic field $B_y x \boldsymbol{e_y}$ in the reconnected plane (x, y)) gives $\boldsymbol{\nabla} \times (\boldsymbol{u} \times \boldsymbol{B}) + \eta \boldsymbol{\Delta B} \sim 0 \Rightarrow (u_{in} B_y/l) \sim \eta (B_y/l^2) \Rightarrow u_{\mathrm{in}} \sim \eta/l$. From these evaluations, one can express l as $l = (\eta L/u_{\mathrm{out}})^2$. It results that $\tau_{RM} \sim \eta^{-1/2} u_{\mathrm{out}}^{-1/2} L^{3/2}$. To express u_{out}, the fluid momentum equation as well as the Ampère–Maxwell equation in the ideal region (meaning that the total magnetic field $\boldsymbol{B} = B_z \boldsymbol{e_z} + B_y x \boldsymbol{e_y}$ has to be considered) are used to give

$$\rho \frac{u_{\mathrm{out}}}{T} \sim \frac{B^2}{\mu_0 L} \Rightarrow \rho \frac{u_{\mathrm{out}}^2}{L} \sim \frac{B^2}{\mu_0 L} \Rightarrow u_{\mathrm{out}} \sim \frac{B}{\sqrt{\rho \mu_0}} = v_A, \tag{2.11}$$

where v_A is the well-known Alfvén velocity. Thus, the flow is driven out of the resistive layer with the Aflvèn velocity. Finally, using the characteristic Alfvén time definition $\tau_A = L/\tau_A$ and the definition of the characteristic resistive time $\tau_\eta = L^2/\eta$, the characteristic reconnection time based on the Sweet–Parker model can be expressed as

$$\tau_{RM} \sim \sqrt{\tau_\eta \tau_A}. \tag{2.12}$$

2.2.2. *Origin of magnetic reconnection in TCV, WEST and JET*

In the past, evaluations of the reconnection time τ_{RM} (2.12) have been done taking L as the ideal macroscopic length scale (i.e. corresponding to a fraction of the tokamak minor radius $\sim$ of a few centimetres) leading to the conclusion that resistive magnetic reconnection cannot occur in a fusion device: due to the high core temperature, the weak resistivity gives a resistive time $\tau_\eta = L^2/\eta$ and, as a consequence, a reconnection time τ_{RM} too long compared with experimental observations. Such evaluations of τ_{RM} for three modern tokamaks of various sizes (small size, TCV; medium size, WEST; large size, JET) can be found in table 1 (third column).

It is interesting to discuss these evaluations. Indeed, these are based on the Sweet–Parker model which is a resistive and steady-state model, where reconnection occurs in the resistive layer and where the drive of the reconnected structure is outside the resistive layer and is led by the ideal induction term $\boldsymbol{u} \times \boldsymbol{B}$. From that picture, the result obtained for the expression of the reconnection time (2.12) is suitable: τ_{RM} is naturally derived from the mechanism inside the resistive layer, i.e. τ_η, and from the mechanism outside the resistive layer i.e. τ_{v_A}. However, one can imagine that once the magnetic reconnection is initiated in the resistive layer of radial size l, other physical mechanisms than the induction field can drive the reconnection structures outside the layer (see § 3). In this new paradigm, the evaluation of the resistive time has to be done taking in consideration the resistive layer size l instead of the macroscopic size L, i.e. $\tau_\eta^l \sim l^2/\eta$. Considering τ_η^l, a new evaluation of

https://doi.org/10.1017/S0022377824001363 Published online by Cambridge University Press

τ_{RM} has been done for the three modern tokamaks in the fourth column of table 1. A better agreement with observations is found. Thus, one can argue that in modern tokamaks, resistive reconnection can occur with reasonable characteristic time in a thin non-ideal layer. The question is then to find relevant mechanism(s) that drive(s) the reconnected structures (i.e. magnetic islands) outside the layer. From this analysis, one can define a new general characteristic reconnection time as $\tau_{RM} \sim \sqrt{\tau^{l}_{\text{origin}}\tau^{L}_{\text{drive}}}$. Here, τ^{l}_{origin} is the characteristic time of the physical process that originates from magnetic reconnection by breaking the frozen-in law on the typical length scale l. Additionally, τ^{L}_{drive} is the characteristic time of the driving physical process that plays a role on the typical length scale L. In the case where resistivity is at the origin of magnetic reconnection, $\tau^{l}_{\text{origin}} = \tau^{l}_{\eta}$.

In the same spirit, although the reconnection process due to electron inertia (see (2.7)) is faster (an evaluation of the characteristic reconnection time based on electronic inertia for modern tokamaks gives $\tau^{m_e}_{RM} \sim L\tau_A/d_e \sim 10^{-3}$ s), it was considered as non-relevant in fusion devices. Indeed, the resulting reconnected structures are too small (of the order of the electron skin depth d_e) compared with the centimetre magnetic islands observed. However, in light of the above, one can consider electronic inertia as a source of possible magnetic island(s) in modern fusion devices: after a initiating phase of magnetic reconnection at small scale due to electronic inertia, another mechanism can drive island(s) outside the non-ideal layer. In this case, one can define the characteristic reconnection time as $\tau_{RM} \sim \sqrt{\tau^{d_e}_{\text{origin}}\tau^{L}_{\text{drive}}}$.

3. Drive

One can conclude from the previous section that resistivity (as well as electronic inertia) can be relevant for modern fusion devices to originate in the required parallel electric field to lead to magnetic reconnection. Following the recipe of the life of a magnetic island, after the original breaking comes the question of the drive. In fusion devices, various physical mechanisms can drive the magnetic reconnection process and accelerate the magnetic island growth. Here, a non-exhaustive inventory of possible mechanisms at play driving the magnetic reconnection process at large scale (§ 3.1) and at small scale (§ 3.2) is presented. The relevance of these mechanisms for fusion devices is discussed.

3.1. *Mechanisms driving large-scale magnetic island*

3.1.1. *Tearing mode, TM*

The Sweet–Parker mechanism presents a physical picture of steady-state and resistive magnetic reconnection. The first linear analysis of unsteady reconnection can be found from Furth, Killeen & Rosenbluth (1963), where the linear investigation of finite resistive instabilities in a current sheet pinch is proposed for the first time. In particular, the linear dispersion relation is derived for the so-called tearing mode. The tearing mode instability is the dynamical extension of the Sweet–Parker model where the resistivity originates in magnetic reconnection in the current layer of size l and drives the growth of the island outside the layer of size L thanks to the mechanism proposed by Sweet and Parker, i.e. thanks to the ideal incoming flow that 'pushes' the magnetic field line towards the null magnetic field line.

To investigate the linear tearing instability, one can consider a simple 3-D slab configuration of a current sheet as seen in § 3 (figure 5), where $\boldsymbol{B} = B_z\boldsymbol{e_z} + B_y\boldsymbol{e_y} + B_x\boldsymbol{e_x}$ with a strong guide field in the $\boldsymbol{e_z}$ direction having $B_z \gg B_y$ and $B_z \gg B_x$. In such a configuration, the presence of a resistive layer (where $\eta \neq 0$) induces the existence of a current sheet in the perpendicular (to the guide field $B_z\boldsymbol{e_z}$) plane (x, y) due to the parallel

https://doi.org/10.1017/S0022377824001363 Published online by Cambridge University Press

current $j_z \boldsymbol{e}_z$ with $j \equiv j_z(x, y)$. Under particular conditions that will be developed just after, such a current sheet can be unstable from the tearing instability point of view: in the perpendicular plane, magnetic reconnection can take place and a 2-D magnetic island can grow with the linear tearing growth rate.

To derive this linear growth rate, the magnetohydrodynamic framework can be used to give a reduced (Strauss 1976) model of the dynamical behaviour of the plasma coupled with the magnetic field:

$$\partial_t \psi + [\phi, \psi] = \eta \nabla_\perp^2 \psi, \tag{3.1}$$

$$\partial_t \nabla_\perp^2 \phi + \left[\phi, \nabla_\perp^2 \phi\right] = \left[\psi, \nabla_\perp^2 \psi\right] + \mu \nabla_\perp^4 \phi, \tag{3.2}$$

where μ is the plasma viscosity. Here, all the quantities have been normalized using the Alfvén velocity v_A, a characteristic macroscopic perpendicular length $L_\perp$ and the Alfvén time $\tau_A = L_\perp / v_A$. Equation (3.1) gives the time evolution of the magnetic flux function in the reconnected plane, i.e. $\psi(x, y)$ defined as $\boldsymbol{B} = B_z \boldsymbol{e}_z + \boldsymbol{\nabla} \times (\psi \boldsymbol{e}_z)$ and represents a reduction of Ohm's law. In particular, $\boldsymbol{\nabla}_\perp \psi \equiv j(x, y)$, which is the current in the parallel direction (i.e. along $\boldsymbol{e}_z$) due to the resistivity that breaks the frozen-in law and allows magnetic reconnection. Equation (3.2) gives the time evolution of the electrostatic potential in the reconnected plane, i.e. $\phi(x, y)$ defined from the fluid velocity in the plane (x, y) $\boldsymbol{u}_\perp = -\boldsymbol{\nabla} \times (\phi \boldsymbol{e}_z)$ and represents the momentum equation. (One can emphasize that symbols $[f, g]$ refer to the nonlinearity of the system and are the well-known Poisson bracket with $[f, g] = \partial_x f \partial_y g - \partial_y f \partial_x g$ in such a configuration.)

The linear tearing mode instability of such a current sheet of size (L_x, L_y) can be investigated by linearizing (3.1) and (3.2):

$$\psi\,(x, y, t) = \psi_0\,(x) + \psi_1\,(x,)\exp(\gamma t)\cos\left(k_y y\right), \tag{3.3}$$

$$\phi\,(x, y, t) = \phi_1\,(x)\exp(\gamma t)\sin\left(k_y y\right). \tag{3.4}$$

In (3.1) and (3.2), it has been assumed that the poloidal direction is a periodic direction with $k_y = 2\pi / L_y$ being the poloidal wave number, and that the fields ψ and ϕ vanish at the boundaries of the radial direction. Here, ψ_0 represents the magnetic flux of the equilibrium current sheet. Additionally, the stability of the well-known Harris current sheet (Harris 1962) is investigated, so $\psi_0(x)$ is such that the associated equilibrium magnetic field is $B_0(x) = \psi_0'(x) = \tanh(x/a)$, where a represents the thickness of the magnetic field in the resistive layer. For such a current sheet, $B_0(x = 0) = 0$ and B_0 is going in opposite directions on either side of the $x = 0$ line, which are necessary conditions to have tearing instability. For a linear unstable current sheet, the fluctuations ψ_1 ($\ll \psi_0$) and ϕ_1 grow exponentially with a linear growth rate γ.

To derive the linear dispersion relation of the tearing mode instability (considering the non-viscous case where $\mu = 0$), the domain has to be separated into an ideal region, where $\eta = 0$, and a resistive region. The asymptotic matching between the two regions leads to this linear dispersion relation.

In the ideal region (labelled as the outside region) of characteristic radial size L, resistivity is neglected $\eta = 0$. Using the decomposition given by (3.3) and (3.4), the linearization of Ohm's law (3.1) leads to the following coupling $\phi_1^{out}(x) = \psi_1^{out}(x)/B_0(x)$. Moreover, it is supposed that the linear growth rate of the tearing mode γ is relatively weak compared with the Alfvén time leading to $1 \ll \gamma \ll \tau_\eta / \tau_A$ and to $\partial_t \nabla_\perp^2 \phi \sim 0$ in (3.2). Thus, under this assumption and using (3.3) and (3.4), the linearization of (3.2)

https://doi.org/10.1017/S0022377824001363 Published online by Cambridge University Press

leads to

$$\left[\psi_0 + \psi_1^{\text{out}} \cos\left(k_y y\right), \nabla_\perp^2 \left(\psi_0 + \psi_1^{\text{out}} \cos\left(k_y y\right)\right)\right] = 0, \tag{3.5}$$

$$\psi_1^{''\text{out}}(x) = \left(\frac{\psi_0^{'''\text{out}}(x)}{B_0(x)} + k_y^2\right) \psi_1^{\text{out}}(x), \tag{3.6}$$

which, for fields vanishing at the the radial boundaries and Harris current sheet, the solution is

$$\psi_1^{\text{out}}(x) = \exp(-k_y|x|) \left[1 + \frac{\tanh \dfrac{|x|}{a}}{ak_y}\right]. \tag{3.7}$$

Due to the presence of the resonant surface where $\eta \neq 0$, this solution presents a discontinuity at $x = 0$ from which the well-known index stability parameter Δ' is defined:

$$\Delta' = \lim_{x \to 0} 2\psi_1^{'\text{out}}(x). \tag{3.8}$$

Finally, for a Harris current sheet and assuming that the fields (ψ and ϕ) vanish at the radial boundaries, one can derive

$$\Delta' = 2\left(\frac{1}{a^2 k_y} - k_y\right). \tag{3.9}$$

It is important to note that Δ' is entirely defined from the outside solution ψ_1^{out}, which is entirely defined by the equilibrium magnetic field in the ideal region. Here, Δ' does not depend at all on the mechanism that originates in the magnetic reconnection (i.e. resistivity or electronic inertia).

In the thin resistive layer (labelled as the inside region) of characteristic radial size l, the resistivity cannot be neglected any longer. Moreover, due to the large scale involved in the linear tearing mode, it is assumed that radial gradients are larger than poloidal gradients leading to $\nabla_\perp^2 \sim \partial_x^2$. It is also assumed that in these non-ideal regions, $\psi_1(x)$ is constant having non-zero derivatives (this is the well-known 'constant-ψ approximation' Furth *et al.* 1963). Then, a Taylor development around $x = 0$ is done to derivate $\psi_0'(x) = B_0(x) \sim -x/a$ for a Harris current sheet. Following these assumptions, the linearization of (3.1) and (3.2) using (3.3) and (3.3) leads to a reduction of the system to an equation independent of the physical parameters:

$$z + z^2 \chi(x) = \chi''(z), \tag{3.10}$$

with $x = (\eta\gamma)^{1/4}\sqrt{a/k_y}\mathrm{z}$ and $\phi_1^{\text{in}}(z) = (\eta\gamma)^{-1/4}\sqrt{k_y a}\chi(z)$, and which is the linearized Ohm's law (3.1). The coupling between ψ and ϕ is given by the linearized momentum equation (3.2):

$$\psi_1^{''in}(x) = \frac{\gamma^2 a}{k_y^2 x}\phi_1^{''\text{in}}(x). \tag{3.11}$$

Finally, the linear dispersion relation is derived from the matching between the two regions and using the definition of Δ' from the ideal region (3.8):

$$\Delta' = \Delta'(\psi_1^{\text{out}}) = \int_{\text{in}} \frac{\psi_1^{''\text{in}}(x)}{\psi_1(0)}\,\mathrm{d}x. \tag{3.12}$$

https://doi.org/10.1017/S0022377824001363 Published online by Cambridge University Press

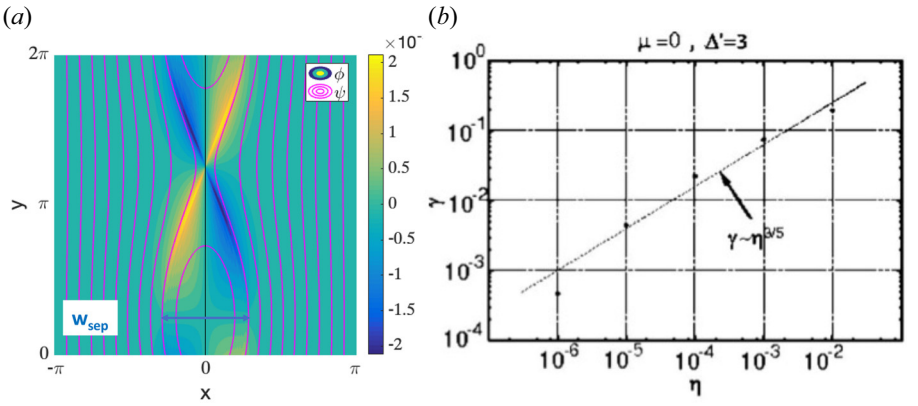

FIGURE 6. (*a*) Scaling law of the linear resistive tearing mode, reproduced from Takeda *et al.* (2008), with permission from AIP Publishing. (*b*) Structure of the fields ψ and ϕ resulting from a tearing instability in the (x, y) reconnected plane.

This matching condition can be solved by deriving a solution for $\psi_1'^{\text{in}}(x)$ from (3.10) and (3.11), and leads to the following expression of the tearing mode linear growth rate:

$$\gamma = 2.13 \Delta'^{5/4} \eta^{3/5} \left(\frac{a}{k_y} \right)^{-2/5}. \tag{3.13}$$

Thus, the Harris current sheet is tearing unstable for $\Delta' > 0$. It is said that Δ' represents the magnetic energy available in the ideal region for instability. During the magnetic reconnection process, the magnetic energy stored in the equilibrium is converted into kinetic energy. As expected, (3.13) shows that the linear drive of the tearing magnetic island is resistive. Figure 6(*b*) (from Takeda *et al.* 2008) shows the scaling law in resistivity of a linear tearing mode for linear simulations of (3.1) and (3.2), and is in agreement with (3.13). It is interesting to note that the linear dispersion relation (3.13) has been obtained here for a resistive tearing mode by considering the asymptotic matching of the ideal region (which does not depend on the physics of the non-ideal layer) with a resistive layer. As a consequence, the linear growth rate γ is a function of the resistivity η. For a collisionless tearing mode, the solution in the ideal region is unchanged, i.e. the expression for Δ' given by (3.9) is still valid. However, the asymptotic matching with the non-ideal layer originating from the electron inertia gives a different linear dispersion relation for the tearing growth rate γ that depends on the electron skin depth. A detailed derivation of the growth rate of the collisionless tearing mode can be found from Porcelli (1991) and Porcelli *et al.* (2002).

The linearization of (3.1) and (3.2) leads to a characteristic radial parity of the tearing mode and the associated flow. In figure 7(*a*), which shows the radial structure obtained numerically of the fields, the tearing mode $\psi_1(x)$ is even while $\phi_1(x)$ is odd. Figure 6(*b*) shows in the (x, y) reconnected plane, the structure of the fields ψ and ϕ resulting from a tearing instability. The dynamic of the flow (through ϕ) and the magnetic field (through ψ) are strongly coupled. The characteristic quadrupole structure observed on ϕ is essential to understand the drive of the magnetic island observed on ψ.

Except during the initial phase, where the current is increased to set the plasma discharge, the tearing instability is usually not observed in modern fusion devices since $\Delta' < 0$. Moreover, the drive of the tearing instability is led by the resistivity. As a

https://doi.org/10.1017/S0022377824001363 Published online by Cambridge University Press

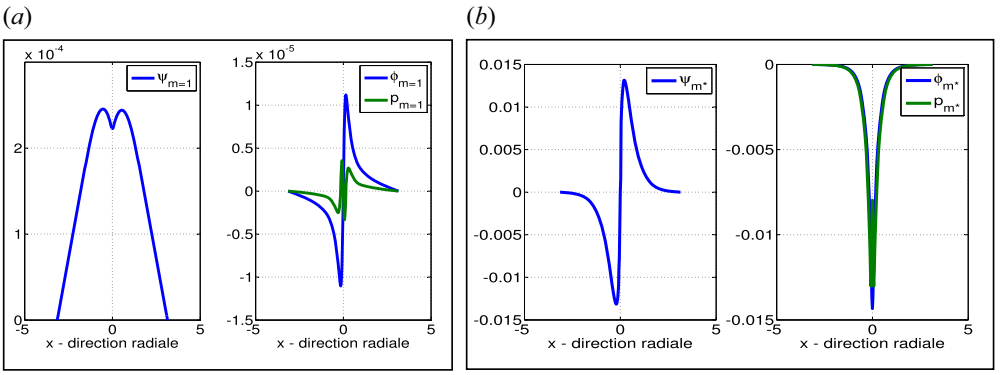

FIGURE 7. (*a*) Radial structure of the fields for a mode (at large scale $m = 1$) having a tearing parity. (*b*) Radial structure of the fields for a mode (at small scale $m* = 33$) having an interchange parity.

consequence, even with an unstable magnetic equilibrium (with $\Delta' > 0$), the resulting growth of a magnetic island due to tearing instability would be too slow compared with the characteristic discharge time of a fusion device. Although the tearing instability is not relevant to explain the existence of magnetic island(s) in modern fusion devices, its study is meaningful and it is useful to understand the physical mechanisms at play during magnetic reconnection processes.

3.1.2. *Neoclassical tearing mode, NTM*

In fusion devices, neoclassical effects through the bootstrap current lead to a physical mechanism that can drive nonlinear large-scale magnetic islands that are deleterious for confinement and transport. Such 'neoclassical tearing modes' (NTMs) (Chang *et al.* 1995; La Haye 2006; Sauter *et al.* 2010) can become very large quickly and reach the tokamak wall bringing with it fast and hot particles which can damage the device. More precisely, the toroidal shape of the tokamak leads to a non-uniform magnetic field in the poloidal direction. Such a magnetic configuration exhibits two classes of trajectory for particles: passing particles that travel all around the torus and trapped particles that are confined in a smaller device region following their well-known 'banana' orbits. The bootstrap current results from the friction between trapped and passing particles. It has been empirically defined as the current carried by the passing electrons and proportional to the radial electronic pressure gradient (resulting from the collisions between the passing electrons and the trapped particles): $j_{BS} = C_b \partial_x p(x)$, where C_b represents the strength of the bootstrap current (Militello, Ottaviani & Porcelli 2008). From that definition, the mechanism at play in the nonlinear drive of a large magnetic island by the bootstrap current can be drawn. A seed magnetic island (see later for the origin of such an island) initially flattens the pressure profile (Fitzpatrick 1995) leading to a perturbation of the bootstrap current. This perturbation amplifies the magnetic island that grows until a fully flattened pressure profile is obtained (at saturation of the island width). Such nonlinear dynamics is well described by the so-call Rutherford model that will be investigated in § 4. To investigate numerically the drive of a magnetic island by the bootstrap current, an heuristic simple model can be derived in the (x, y) reconnected plane using the reduced-MHD

https://doi.org/10.1017/S0022377824001363 Published online by Cambridge University Press

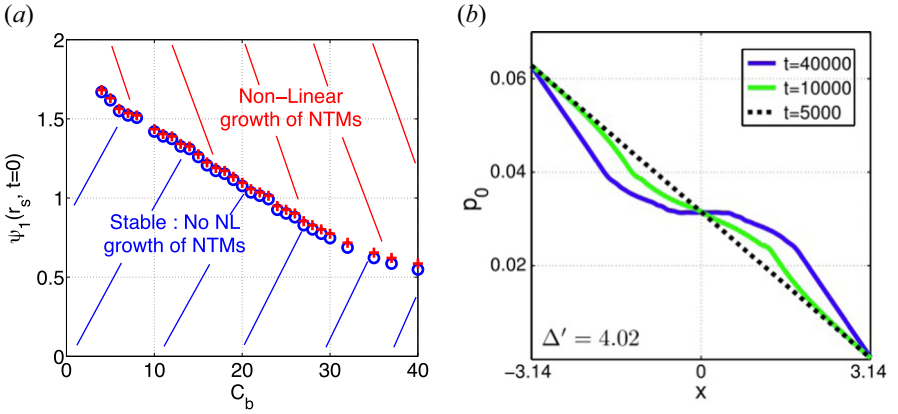

FIGURE 8. (*a*) NTM stability diagram obtained thanks to nonlinear simulations of (3.14)–(3.16). (*b*) Pressure profile $P_0(x)$ is flattened while the NTM island grows (reproduced from Agullo *et al.* (2014), with permission from AIP Publishing).

framework and giving the following time evolution equations (Muraglia *et al.* 2017):

$$\partial_t \psi + [\phi - P, \psi] = -v^\star \partial_y \psi + \eta \nabla_\perp^2 \psi + \eta C_b \partial_x P, \tag{3.14}$$

$$\partial_t \nabla_\perp^2 \phi + \left[\phi, \nabla_\perp^2 \phi\right] = \left[\psi, \nabla_\perp^2 \psi\right] + \mu \nabla_\perp^4 \phi, \tag{3.15}$$

$$\partial_t P + [\phi, P] = -v^\star \partial_y \phi + \rho^{\star^2} \left[\psi, \nabla_\perp^2 \psi\right] + \chi_\perp \nabla_\perp^2 P. \tag{3.16}$$

Equation (3.16) gives the time evolution of the electronic pressure P with $v^\star$ being the electronic diamagnetic velocity induced by the equilibrium electronic pressure (i.e. at the equilibrium $\partial_x P_0(x) = v^\star$). Here, $\rho^\star$ is the normalized ionic Larmor radius and $\chi_\perp$ is the perpendicular conductivity. The model contains implicitly a parallel conductivity through the coupling between (3.14) and (3.16) given by $\chi_\parallel = \rho^{\star^2}/\eta$ (Agullo *et al.* 2014). This term is required to initiate the pressure flattening inside the island when its radial width becomes larger than (Fitzpatrick 1995)

$$w_c = \sqrt{8}\left(\chi_\perp/\chi_\parallel\right)^{1/4} \sqrt{a/k_y}. \tag{3.17}$$

In fusion devices, the nonlinear drive of a magnetic island by the bootstrap current requires a seed island of radial width w_{seed} (which is not usually originated from the tearing instability since $\Delta' < 0$). The NTM triggering is a threshold mechanism: for a given bootstrap current (of strength C_b), w_{seed} has to be large enough to initiate the NTM mechanism. This is well observed in figure 8(*a*) that shows the NTM stability diagram obtained thanks to nonlinear simulations of (3.14)–(3.16). In these simulations, $\Delta' < 0$ and the required seed island of radial width w_{seed} is numerically implemented in the initial conditions of the simulations. In figure 8(*b*) taken from Agullo *et al.* (2014), the evolution of the pressure profile during the nonlinear NTM growth is shown. Once the island width reaches the critical width w_d, the pressure profile starts to become flat inside the island until the saturation phase where the island width saturates and the pressure profile is completely flattened.

3.1.3. *Turbulence driven magnetic island, TDMI*

NTM requires a seed magnetic island which is amplified by the bootstrap current. Some 'NTM precursors' have been identified in experiments. For example, sawtooth crashes,

https://doi.org/10.1017/S0022377824001363 Published online by Cambridge University Press

fishbone instabilities or edge-localized modes are some possible MHD events that can generate the required seed magnetic island. However, the basic physical mechanism at play in the seed island generation is still not understood. Moreover, in some discharges, in particular, in high-poloidal-beta discharges, NTMs are observed without any MHD precursor events (Isayama *et al.* 2013). Thus, many questions related to the NTMs origin are still open. In hot fusion plasmas, large-scale MHD structures (like magnetic islands) co-exist with small-scale turbulence. The recent work in the tokamak KSTAR (Choi *et al.* 2021) shows the existence of a mutual interaction between turbulence and the magnetic island. Naturally, the small-scale turbulence could be one candidate to explain the origin of the seed island required for NTM. In this last decade, several theoretical works have addressed the question of the role of turbulence in the seed island generation. One of the main results is that a magnetic island can be driven by small-scale turbulence and such an island is called a turbulence driven magnetic island (TDMI) (Muraglia *et al.* 2011). Here, the physical mechanism at play in the drive of a TDMI is presented as well as a review of works devoted to TDMI.

Muraglia *et al.* (2009*a*,*b*) derived a reduced-MHD model for the multi-scale interaction of a large magnetic island and interchange small-scale turbulence. Typically, this model describes in the 2-D reconnected plane (x, y) the nonlinear time evolution of the magnetic flux ψ, (3.18), of the electric potential ϕ, (3.19), and of the electronic pressure P, (3.20):

$$\partial_t \psi + [\phi - P, \psi] = -v^\star \partial_y \psi + \eta \nabla_\perp^2 \psi, \tag{3.18}$$

$$\partial_t \nabla_\perp^2 \phi + [\phi, \nabla_\perp^2 \phi] = [\psi, \nabla_\perp^2 \psi] - \kappa_1 \partial_y P + \mu \nabla_\perp^4 \phi, \tag{3.19}$$

$$\partial_t P + [\phi, P] = -v^\star((1-\kappa_2)\partial_y \phi + \kappa_2 \partial_y P) + \rho^{\star^2}[\psi, \nabla_\perp^2 \psi] + \chi_\perp \nabla_\perp^2 P. \tag{3.20}$$

This model includes both the tearing physics through the magnetic equilibrium shaped with a Harris current sheet (i.e. having $\boldsymbol{B_0}(x) = \tanh((x - L_x/2)/a)\boldsymbol{e_y}$) and the interchange physics through κ_1 and κ_2 terms. Indeed the κ_1 represent the magnetic curvature and the κ_2 and $v^\star$ parameters represents the equilibrium pressure gradient. When the curvature is in opposition with this gradient, interchange instability develops at small scales.

Like for the linear tearing mode, in the box $([-L_x/2, L_x/2], [0, L_y])$, the fields are considered as periodic in the poloidal direction (i.e. in the y-direction) and vanish at the radial boundaries. Therefore, one can decomposed the fields (ψ, ϕ and P) using a Fourier decomposition with some of the poloidal modes m: $\psi(x, y, t) = \sum_{m\in\mathbb{Z}} \psi_m(x, t) \exp(\mathrm{i}k_m y)$ with $k_m = 2\pi m/L_y$. The parity, i.e. odd or even symmetry in the radial direction, of the eigenfunctions $\psi_m(x, t)$, $\phi_m(x, t)$, $P_m(x, t)$ provides a distinct marker of identification of a given mode m and helps to pinpoint the instability mechanism generating it. Small-scale interchange modes have (odd, even, even) parities with respect to $x \in [-L_x/2, L_x/2]$ for (ψ_m, ϕ_m, P_m), respectively. Usually, interchange modes are unstable at small scales, i.e. $m \gg 1$. Tearing mode has (even, odd, odd) parities with respect to $x \in [-L_x/2, L_x/2]$ for (ψ_m, ϕ_m, P_m), respectively. Usually, the tearing mode is unstable at large scales, i.e. $m \sim 1$ (see figure 7).

To understand how unstable interchange modes at small scales can drive the growth of an $m = 1$ magnetic island, one can consider the linear spectrum with $C_b = 0$ (blue crosses) presented in figure 9(*a*). This spectrum is obtained by a linear simulation of (3.18), (3.19) and (3.20) using parameters such as at large scales, all the modes are stable and at small scales, the modes are unstable. In particular, at small scales, the unstable modes present an interchange parity and the most unstable mode is $m^\star = 33$ with a linear growth rate $\gamma^\star$. At large scale, the mode $m = 1$ is stable and presents an interchange parity with $\Delta' < 0$. Thus, linearly, there is no magnetic island. Then, from this linear spectrum, nonlinear

https://doi.org/10.1017/S0022377824001363 Published online by Cambridge University Press

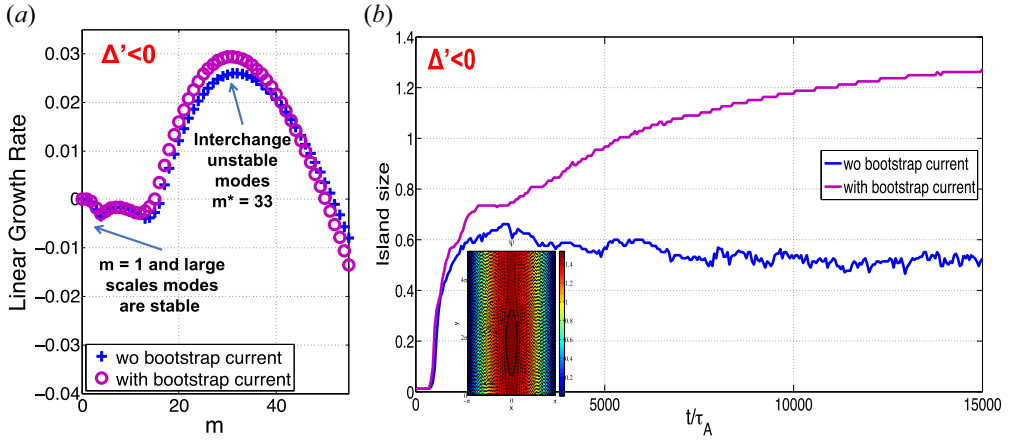

FIGURE 9. (*a*) Linear spectrum of a typical TDMI simulation. Two cases are considered: without bootstrap current, i.e. $C_b = 0$ (blue crosses) and with bootstrap current, i.e. $C_b = 40 \neq 0$ (purple circles). (*b*) Nonlinear TDMI simulations with $\Delta' < 0$ without (blue line) and with (magenta line) bootstrap current.

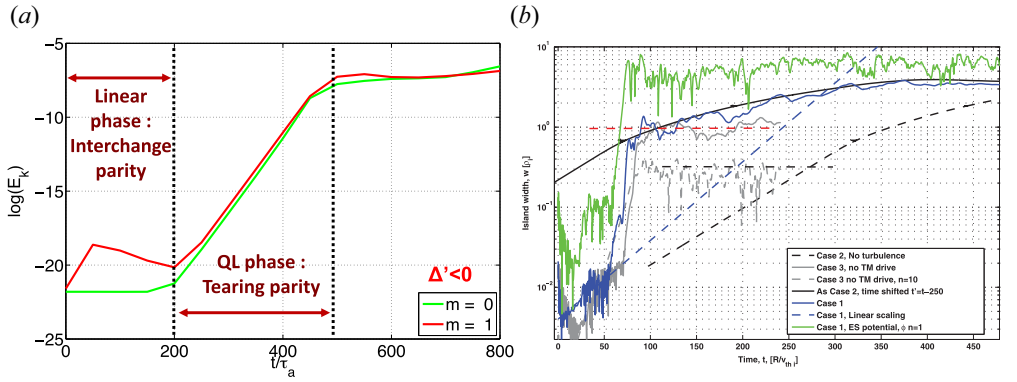

FIGURE 10. (*a*) TDMI generation mechanism. Time evolution of the kinetic energy of the large-scale modes $m = 1$ and $m = 0$ at the beginning of the nonlinear simulation. (*b*) Hornsby *et al.* (2016) observe TDMI in global gyrokinetic simulations including collisions. Ion temperature gradient (ITG) turbulence accelerates the growth of a resistive tearing mode following the rule $\gamma_1^{NL} \sim 2\gamma^\star$.

simulation is performed without bootstrap current (i.e. $C_b = 0$) and the nonlinear growth of a $m = 1$ magnetic island is observed whereas $\Delta' < 0$. Indeed, figure 9(*b*) gives the time evolution of the island for a nonlinear simulation with $\Delta' < 0$ and without bootstrap current (i.e. $C_b = 0$ with the blue line). The contour plot of $\psi + \psi_0$ at the end of the simulation is shown and exhibits a magnetic island in figure 9(*b*). This magnetic island has been nonlinearly generated thanks to the nonlinear interaction between small scales and large scales (Muraglia *et al.* 2011).

The time evolution of the kinetic energy of the large-scale modes $m = 0$ and $m = 1$ for the nonlinear simulation with $\Delta' < 0$ and $C_b = 0$ is presented in figure 10(*a*). It clearly reveals that the beginning of the simulation can be decomposed into three phases.

https://doi.org/10.1017/S0022377824001363 Published online by Cambridge University Press

First, for $t/\tau_A = [0, 200]$, there is the linear phase which is in agreement with the linear spectrum presented in figure 9(*b*): the modes $m = 0$ and $m = 1$ are stable and present an interchange parity. There is no magnetic island. Around the resonance surface $x = 0$, small-scale modes grow.

Then, the second phase ($t/\tau_A = [200, 500]$ in figure 10*a*) is quasi-linear: a positive growth with $\gamma_0^{NL} \sim \gamma_1^{NL} \sim 2\gamma^\star$ of the large-scale modes $m = 0$ and $m = 1$ is observed. During this phase, the parity of the large-scale modes $m = 0$ and $m = 1$ change into a tearing parity: the magnetic island is generated. Using the parity properties of the system, one can explain the physical mechanism at play during this phase where the TDMI is generated. Indeed, at small scales, the two most interchangeable unstable modes $m^\star$ and $m^\star + 1$ with a comparable linear growth rate $\gamma^\star$ (see figure 9*a*) beat together to drive nonlinearly a magnetic island with $\gamma_1^{NL} \sim 2\gamma^\star$. This nonlinear beating is dominant in the simulation dynamics and leads to a change of parity of the modes $m = 0$ and $m = 1$. Indeed, the nonlinear properties of (3.18), (3.19) and (3.20) are such that if the system is linearly driven by small-scale (ss) interchange modes I_{ss}, their mutual nonlinear interaction can drive only a tearing parity large-scale (ls) fluctuation T_{ls}: $[I_{ss}, I_{ss}] \to T_{ls}$. More precisely, the projection of Ohm's law (3.18) on the mode $m = 1$ illustrates the nonlinear beating at small scales of the interchange modes driving a tearing parity mode at large scale: $\partial_t \psi_1 \sim [\psi_{m^*}, \phi_{m^\star+1} - p_{m^\star+1}] + \eta \nabla_\perp^2 \boldsymbol{\psi_1}$ (Muraglia *et al.* 2011; Ishizawa *et al.* 2019).

Finally, up to $t/\tau_A > 500$ (figure 10*a*), the system enters into a fully nonlinear regime and the island width is saturated as presented in figure 9(*a*) with $C_b = 0$.

Thus, one can conclude that the large-scale magnetic island generated by a nonlinear beating of small-scale unstable interchange modes is a TDMI. The drive of such an island is not governed by the resistivity. However, it is the resistivity that originates in the island by allowing magnetic reconnection. This important result, which was first presented by Muraglia *et al.* (2011) in the MHD context, was recovered later with gyrokinetic simulations (Hornsby *et al.* 2015*b*, 2016) where the ITG turbulence accelerates the growth of a resistive tearing mode following the rule $\gamma_1^{NL} \sim 2\gamma^\star$ (see figure 10*b*).

From this work, the question of the amplification of a TDMI by the bootstrap current to lead to a NTM becomes natural. To answer this question, linear and nonlinear simulations of (3.18), (3.19) and (3.20) including both the bootstrap current ($C_b \neq 0$) and turbulence (i.e. interchange small-scale unstable modes with $\kappa_1 \neq 0$ and $\kappa_2 \neq 0$) have been performed with $\Delta' < 0$. In figure 9(*b*), the linear spectrum of such simulations is presented with purple circles ($C_b = 40$). The bootstrap current does not affect so much the linear spectrum which presents always unstable interchange modes at small scales and stable tearing mode at large scales. Linearly, there is no magnetic island with bootstrap current. Nonlinearly, as presented in blue in figure 9(*a*), without bootstrap current, a TDMI is generated. Additionally, the magenta line shows the time evolution of the island when the bootstrap current is included in the model: the TDMI is amplified by the bootstrap current to lead to an NTM. Thus, one can conclude that the TDMI generation mechanism can explain the origin of the required seed island for the growth of NTM in fusion devices (Muraglia *et al.* 2017).

In the first study by Muraglia *et al.* (2011), the model used is by nature 2-D (in the reconnected plane) with a Cartesian geometry. Moreover, turbulence and island are located at the same resonant surface whereas in fusion devices, magnetic reconnection can take place at a different radial location than that of turbulence. As an example, a sawtooth crash can generate magnetic island in the core of the machine while interchange-like turbulence develops at the device pedestal where gradients are strong. In that context, Poyé *et al.* (2015) investigated the resilience of the TDMI mechanism found by Muraglia

https://doi.org/10.1017/S0022377824001363 Published online by Cambridge University Press

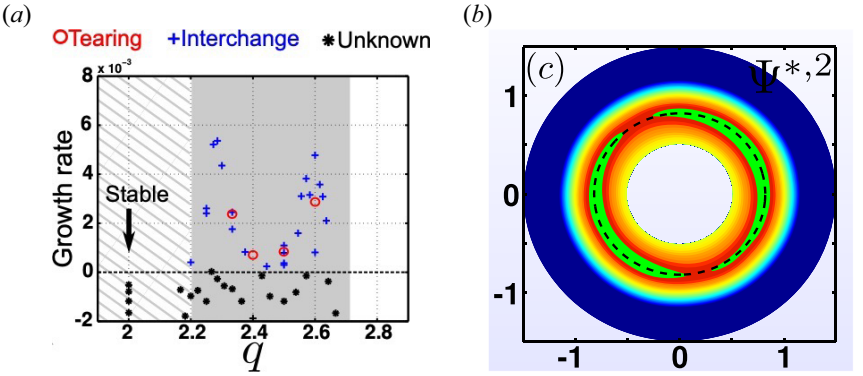

FIGURE 11. (*a*) Linear spectrum as a function of the radial coordinate q used in the 3-D geometrical nonlinear simulations (reproduced from Poyé *et al.* (2015), with permission from AIP Publishing). (*b*) Magnetic flux ψ obtained during the saturation phase of 3-D cylindrical nonlinear simulations (reproduced from Poyé *et al.* (2015), with permission from AIP Publishing).

et al. (2011) using an RMHD framework in 3-D cylindrical geometry in the situation where interchange-like turbulence is located outside the $q = 2$ resonant surface, which is the surface where a large (2, 1) magnetic island is usually observed. One can note that here and in the following, the bootstrap current is not included. In figure 11(*a*), the linear spectrum as a function of the radial coordinate q used in the 3-D geometrical nonlinear simulations of Poyé *et al.* (2015) is shown: the input parameters of the simulations are chosen to have stable tearing mode around the $q = 2$ surface and unstable interchange modes in the region outside the $q = 2$ surface. So linearly, there is no magnetic island. As shown in figure 11(*b*), nonlinearly, a (2, 1) magnetic island is observed on the magnetic flux ψ. Here, after the linear phase, similar to 2-D, an efficient beating between turbulent modes is produced with large tearing radial structure (5, 2), (7, 3) and (9, 4) using the parity rule $[I_{ss,}\ I_{ss}] \rightarrow T_{ls}$. However, those modes are located in the region where the interchange modes are unstable and so outside the $q = 2$ surface. In figflagfigure 12(*a*), the radial structure of these modes is presented and shows that these modes, due to their tearing structure, have an extended radial structure and reach the $q = 2$ surface. Using the parity rule $[T_{ss,}\ T_{ss}] \rightarrow T_{ls}$, these modes beat together nonlinearly at the surface $q = 2$ giving birth to the growth of a $(2:\ 1)$ magnetic island with an interchange characteristic time. From this work (Poyé *et al.* 2015), one can give rules for a 3-D nonlinear coherent and non-local beating for TDMI growth: (1) the modes beat if they overlap; (2) the beating is efficient if the resulting mode is resonant at its birth location.

Dubuit *et al.* (2021) added toroidal effects in the 3-D RMHD model. Two paths towards TDMI are found. The first path, based on linear toroidal coupling, generates a turbulence cascade from small scales to large scales. At small scales, local (as in 2-D) and non-local (as in 3-D cylindrical) turbulence modes cascade together towards the large scale using first the $[I_{ss,}\ I_{ss}] \rightarrow T_{ls}$ rule and then the $[T_{ss,}\ T_{ss}] \rightarrow T_{ls}$ rule to produce a (2, 1) magnetic island. The second path is the nonlinear TDMI generation mechanism already investigated in 3-D cylindrical configuration by Poyé *et al.* (2015). As shown in figure 12(*a*), the width at saturation of the generated (2, 1) TDMI is proportional to the input power source, i.e. to the turbulence level. Moreover, the path chosen by the system to generate the (2, 1) TDMI depends also on the input power. For weak turbulence and input power source, the toroidal linear interaction is dominant and the system follows the first path to generate a

https://doi.org/10.1017/S0022377824001363 Published online by Cambridge University Press

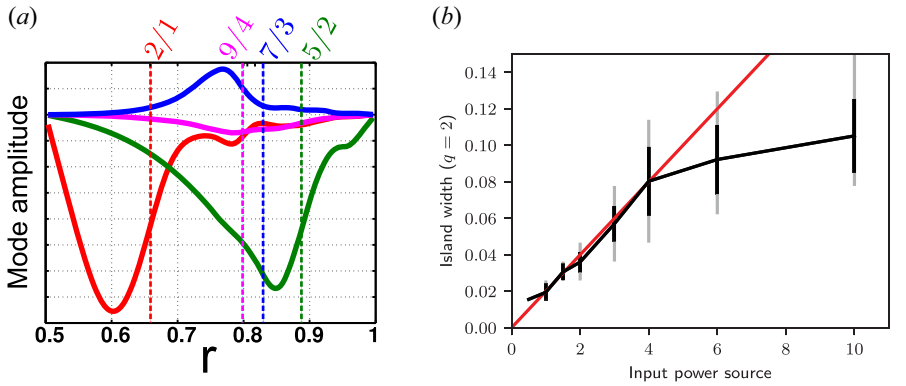

FIGURE 12. (*a*) Radial structure of modes in a 3-D nonlinear simulation of Poyé *et al.* (2015). (*b*) Reproduced from Dubuit *et al.* (2021), with permission from AIP Publishing, it is shown that the saturated width of the (2, 1) TDMI generated in 3-D toroidal configuration is proportional to input power source, i.e. to the turbulence level. One can note that after a input power source > 4, the island becomes too large compared with the size of the numerical box.

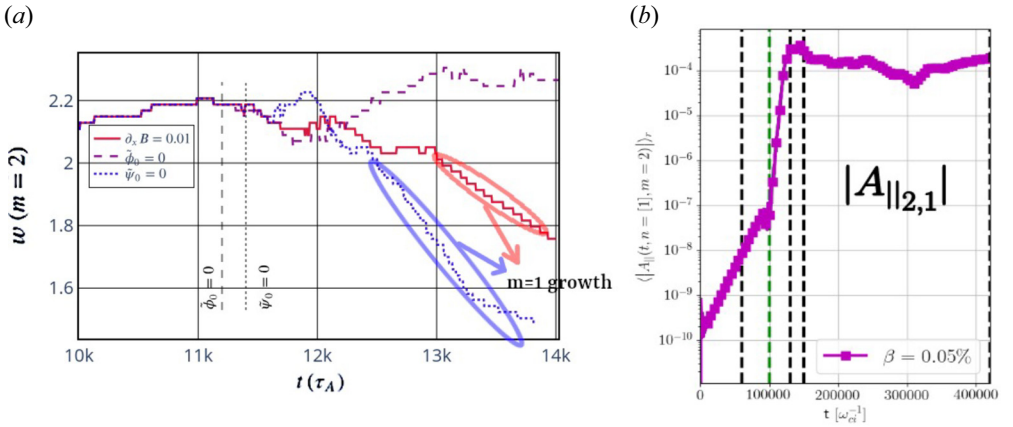

FIGURE 13. (*a*) Nonlinear time evolution of the $m = 2$ mode width in simulations of 2-D and six-fieldsRMHD model (by courtesy of D. Villa *et al.*). (*b*) Time evolution of a (2, 1) magnetic island in PIC and collisionless simulation, and in the presence of ITG turbulence (by courtesy of F. Fidmer *et al.*). Thanks to the electronic inertia, a tearing mode grows linearly at the beginning of the simulation. Then, an acceleration of its growth due to nonlinear beating of ITG modes is observed.

TDMI. When the input power source increases, the nonlinear interactions overcome the linear cascade and the second path is followed.

Recently, in a work just submitted, D. Villa *et al.* used a 2-D and six-fields RMHD model (Frank *et al.* 2020) to find a new path towards TDMI involving coupling between kinetic ballooning modes and zonal flows at low magnetic shear. In figure 13(*a*), the nonlinear time evolution of the $m = 2$ mode width is presented. The kinetic ballooning modes get tearing parity to drive TDMI at the beginning of the nonlinear phase. In the presence of zonal flow, a coalescence of modes towards the $m = 1$ scale with a tearing structure is observed.

https://doi.org/10.1017/S0022377824001363 Published online by Cambridge University Press

In a recent work of F. Widmer *et al.* (that is currently in the process for submission), the acceleration by ITG turbulence of the drive of a tearing mode originated by electronic inertia is observed in PIC and collisionless simulations (figure 13*b*).

Seto *et al.* (2024) used RMHD simulations to find that TDMIs (driven by drift ballooning modes) can be interpreted as ELM precursors and, by consequence, can play a role in the ELM triggering.

More generally, various examples exist in the literature where the magnetic island is driven/accelerated by a physical mechanism that is not the one that initially breaks the frozen-in law. Without being exhaustive, one can quote Ishii, Azumi & Kishimoto (2002), where simulations show that the magnetic reconnection process is accelerated thanks to a nonlinear interaction between two unstable tearing modes. Moreover, in the ELM context, plasmoid-mediated reconnection is observed in MHD simulations of nonlinear peeling–ballooning edge-localized modes (Ebrahimi & Bhattacharjee 2023). Finally, Grasso *et al.* (2020) found by means of RMHD simulations that collisionless magnetic reconnection (originating from electron inertia) can be accelerated in the presence of Kelvin–Helmoltz instability.

Up to now, although the work of Choi *et al.* (2021) shows experimentally the existence of a mutual interaction between turbulence and magnetic island in KSTAR, there is no experimental evidence for the existence of TDMI in modern fusion devices and for the generation of NTM from TDMI. This work is in progress thanks to collaborations between European researchers.

3.2. *Mechanisms driving small-scale magnetic reconnection*

3.2.1. *Relevance of the microtearing mode instability in modern fusion devices*

The microtearing mode (MTM) is another example where a magnetic island is originated from collisions, i.e. resistivity, that allow magnetic reconnection and another physical mechanism to drive the growth of the mode: for MTM, the energy source for the instability is the electron temperature gradient. Here, the mechanisms in the presence of collisions will be highlighted (although an electron temperature gradient can also destabilize MTM originating from electron inertia).

More precisely, microtearing instability corresponds to the destabilization at ion small scales of a collisional current layer by the electron temperature gradient (Hazeltine *et al.* 1975; Drake & Lee 1977). Due to the characteristic length scale $l_{MTM} \sim r_{L_i}$ (where r_{L_i} is the ionic Larmor radius) that is involved in the MTM destabilization mechanisms, the MHD framework is useless to investigate this instability. MTM analysis requires a kinetic or a gyrokinetic framework.

For many years, on the argument that collisions were very weak in a high temperature fusion plasma, MTMs have been the subject of few investigations with the assumption that they were stable in fusion devices. However, in this last decade, several works have found unstable MTMs in gyrokinetic simulations of fusion plasmas. In particular, they were found to be unstable in the pedestal region where the gradients (and of course the electron temperature gradient) are strong. Applegate *et al.* (2007) and Dickinson *et al.* (2013) found unstable MTMs in the pedestal of the spherical tokamak MAST. Doerk *et al.* (2011) found unstable MTMs for standard tokamaks like ASDEX-Upgrade. Then, Predebon & Sattin (2013) found unstable MTMs in reversed field pinches. Later, Hatch *et al.* (2016) observed that unstable MTM were found to play an important role in the pedestal of JET-ILW. Due to their possible impact on the electron heat transport in the pedestal, theses results are very important and lead to open questions. What exactly is the role played by collisions in the MTM destabilization mechanism? Are there other physical mechanisms leading

https://doi.org/10.1017/S0022377824001363 Published online by Cambridge University Press

to an increase of MTMs drive and growth rate? Here, a review of the possible physical mechanisms at play for the drive of the microtearing mode is presented.

3.2.2. *Linear destabilization of a current sheet by MTM*

To illustrate what could be an MTM, the slab configuration of figure 5 can be used. Here again, there is a strong magnetic field in the parallel direction ($\boldsymbol{e}_z$) and the reconnection process takes place in the (x, y) plane. The linear theory of the MTM follows the same procedure as that for the large-scale tearing mode. First, the domain is decomposed into an ideal region and a collisional region.

In the ideal region, there is no current, i.e. $-\mu_0 j_{\parallel \mathrm{out}} = \nabla_\perp^2 \psi_{\mathrm{out}} = 0$. As for the large-scale tearing mode, this leads to $\psi_{\mathrm{out}}(x) \sim \exp^{-k_m|x|}$, where it has been considered that the boundary conditions are far (even at infinity) from the current sheet (which is a good hypothesis for a small-scale MTM). In the collisional region, collisions lead to the formation of a current sheet, where $j_{\parallel in} \neq 0$ and the magnetic flux is assumed to be constant (the so-called 'ψ-constant' approximation already mentioned for the large-scale tearing mode) $\psi_{in} = cte$. Then, the two regions are matched given the expression of the $\Delta'^{MTM}_{k_m}$ parameter:

$$\Delta'^{MTM}_{k_m} = \lim_{L\to 0} \frac{1}{\psi\,(0)} \left.\frac{\mathrm{d}\psi}{\mathrm{d}x}\right|_{-L}^{L} = \int_{-\infty}^{+\infty} \sigma\,(x)\ \mathrm{d}x = -2\,|k_m| < 0, \tag{3.21}$$

where $\sigma(x) = j_\parallel/\psi$ is the kinetic conductivity. Thus, for an MTM, Δ'^{MTM} is always negative. The destabilization is done by the electron temperature gradient which drives the mode.

The kinetic theoretical derivation of the MTM linear dispersion relation has been done by Hamed *et al.* (2019) taking into account collisions as the mechanism allowing for the breaking of the frozen-in law (i.e. originating from the magnetic reconnection process). Note that due to the scales involved, the resolution of the system in the non-ideal layer has to be done using a kinetic framework. Following the Sweet–Parker mechanism, where the coupling between the magnetic field and the flow is an essential key of the dynamics, the electric potential is taken into account in the MTM linear theory through the well-known Maxwell–Gauss equation. The magnetic drift is also added in the evaluation of the collisional Vlasov equation given the time evolution of the electron distribution function f_e. This leads to a derivation of a model that couples the magnetic flux and the electric potential in the reconnected plane. This model is the kinetic equivalent to the reduced-MHD model for the large-scale tearing mode given by (3.1), (3.2) and it is naturally called the kinetic reduced-MHD (KRMHD) model. In the 1-D-1V phase space $(\hat{x}, \hat{v})$, it can be expressed as (Hamed *et al.* 2019)

$$\nabla_\perp^2 \hat{\psi}\,(\hat{x}) + \hat{\beta}\hat{\sigma}_{\omega_d}(\hat{x}, \hat{v})\left(\hat{\psi}\,(\hat{x}) - \frac{\hat{x}}{\hat{\omega}}\hat{\phi}\,(\hat{x})\right) = 0, \tag{3.22}$$

$$\nabla_\perp^2 \hat{\phi}\,(\hat{x}) + \hat{\mu}_e\,(\hat{\omega})\,\frac{\hat{x}}{\hat{\omega}}\hat{\sigma}_{\omega_d}(\hat{x}, \hat{v})\left(\hat{\psi}\,(\hat{x}) - \frac{\hat{x}}{\hat{\omega}}\hat{\phi}\,(\hat{x})\right) - \hat{C}_{int}\hat{\phi}\,(\hat{x}) = 0, \tag{3.23}$$

where $\hat{\beta}$ is the well-known normalized beta parameter, $\hat{\sigma}_{\omega_d}$ is the normalized conductivity that depends on the magnetic drift ω_d (for more details, see (Hamed *et al.* 2019)) and $\hat{\mu}_e$ is a normalized quantity linked to the mass ratio $\frac{m_e}{m_i}$, to the magnetic shear length L_s, to the electron temperature gradient length scale L_{T_e} and to the normalized mode growth and frequency, i.e. $\hat{\omega} = \hat{\omega}_r + i\hat{\gamma}$. Finally, $\hat{C}_{int}$ is a normalized quantity linked to interchange

https://doi.org/10.1017/S0022377824001363 Published online by Cambridge University Press

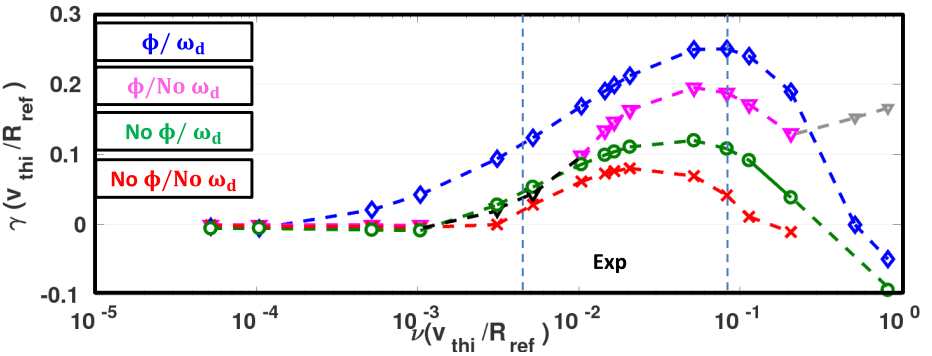

FIGURE 14. Linear destabilization of the microtearing mode: theoretical linear growth rate γ of the mode as a function of collisions ν (reproduced from Hamed *et al.* (2019), with permission from AIP Publishing).

terms. The resolution of the KRMHD model given by (3.22) and (3.23) gives the linear theory of MTM, i.e. the expression of $\hat{\omega}$, and the profile of $\hat{\psi}(\hat{x})$ and $\hat{\phi}(\hat{x})$.

3.2.3. *Impact of the electric potential and of the magnetic curvature on the MTM drive*

To investigate the mechanisms at play in the MTM drive, the KRMHD model given by (3.22) and (3.23) can be solved by using an eigenvalue code (here the SolveAP code) taking into account the boundary conditions.

figure 14 represents the theoretical linear growth rate γ as a function of the collisions ν for different models. Whatever the models used, the microtearing mode is stable in the absence of collisions. As expected, collisions are the mechanism that originates in the reconnection process. Although collisions are weak in a fusion device, they are strong enough to allow magnetic reconnection (the vertical blue dash lines in figure 14 give the experimental range for the collisions in the JET-ILW pedestal). Then, another physical model drives the growth of the island. To investigate the possible mechanisms at play in the drive of MTM, various models have been tested in figure 14.

The most simple model is represented by the red crosses, where the electrostatic field and the magnetic drift have been removed from the model. In the absence of an electric potential, the required coupling between the magnetic field and the plasma flow is assured by the electronic pressure through the distribution function of the electrons (Muraglia *et al.* 2009*a*). In this model, the electron temperature gradient drives the MTM growth as in the past work of Hazeltine *et al.* (1975) and Drake & Lee (1977). The impact of the electric potential and the magnetic drift on the MTM drive is investigated by Hamed *et al.* (2019), as shown in figure 14. The green circles show the linear MTM growth rate using a model without electric potential and including the magnetic drift. The magenta triangles show the growth rate for a model without the magnetic drift and with the electric potential. Finally, the blue diamonds show the result for a model including both. One can conclude that the electric potential and the magnetic drift do not destabilize MTM at the low collisional regime, and in the presence of collisions, they amplify the MTM drive by the electron temperature gradient and collisions.

It is interesting to highlight that here, the drive of MTM has been addressed only in a linear regime. However, nonlinear interactions with others (turbulent) modes can affect the nonlinear growth of MTMs. In particular, Maeyama, Watanabe & Ishizawa (2017) showed

https://doi.org/10.1017/S0022377824001363 Published online by Cambridge University Press

that MTMs can be suppressed in the presence of electron temperature gradient (ETG) modes.

4. Saturation

The last step of an island life is its saturation: an island grows until it reaches its saturated width. The understanding of the saturation mechanisms at play for magnetic reconnection at large scales (or at small scales) is fundamental to understand the impact of the island(s) on the magnetic confinement. This last section is dedicated to a review of the last results on the theoretical understanding of saturation of a large-scale magnetic island (without and with bootstrap current).

4.1. *Understanding of large-scale tearing magnetic island saturation*

4.1.1. *History of Rutherford-like models and magnetic island width definition*

To limit the impact of a large-scale NTM island, a theory on the saturation mechanisms of tearing has emerged over the last decade giving a variety of Rutherford-like models. From Ohm's law, (3.1) or (3.14), these models give a zero-dimensinoal (0-D) time evolution equation of the island radial width from which the width at saturation w_{sat} can be predicted (Rutherford 1973). Naturally, these models have been largely used in experiments to control and reduce the width of a NTM(s) (Sauter *et al.* 2010; Kong *et al.* 2022, 2020) (see figure 15*b*). However, up to now, systematic comparisons of Rutherford-like models with numerical simulations evolving NTM have failed. Militello *et al.* (2008) performed one of the first works dedicated to validation of Rutherford-like model with simulations using the reduced-MHD model (similar to (3.14), (3.15) and (3.16)). As shown by figure 16(*a*), in this work, only the prediction of the saturated island width, and not the complete dynamics, has been investigated and good agreement is found with theory only in the case of the metastable magnetic island having a small saturated island width. Later, the work of Maget *et al.* (2016) used an extended MHD model to investigate NTM computations to test the validity of the Rutherford-like model including bootstrap current (Carrera *et al.* 1986). Agreement is found only by adjusting empirically the theoretical model (by adjusting what will be called later 'Rutherford parameters') to numerical results instead of computing these parameters from first principles. In the same way, in the work of Westerhof, Blank & Pratt (2016), based on reduced-MHD simulations, all NTM dynamics is not recovered numerically and only the contribution of the bootstrap current agrees with theory. In fact, to understand the discrepancy between simulations and Rutherford-like models in the prediction of NTM dynamics and saturation, some preliminary steps are required: first, a discussion on the island radial width definition is required, and then, a better understanding of the nonlinear dynamics and saturation of a resistive tearing mode without bootstrap current is required.

First of all, an intuitive definition of the island width can be given from the ψ contour plot in the reconnected plane shown in figure 6(*a*). Indeed, the radial width of the magnetic island can be defined as the radial extension of the island envelop drawn from lines called separatrices. In the following, the island width defined from this method is labelled w_{sep} and can be computed directly from simulations.

Then, Biskamp (2000) gives a first theoretical definition of the radial island width associated to the width of the $m = 1$ mode and labelled w_1:

$$w_1 = 4\sqrt{2a\psi_1^{\mathrm{res}}}, \tag{4.1}$$

which can be computed from the simulations by evaluating ψ_1^{res}.

Finally, following the pioneering work of Rutherford (1973), one can consider that the saturation mechanism is mainly driven by the nonlinear interaction between the unstable

https://doi.org/10.1017/S0022377824001363 Published online by Cambridge University Press

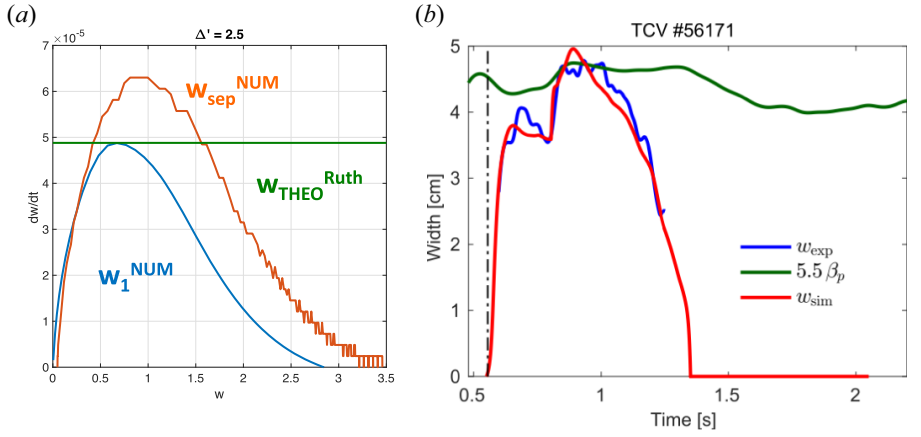

FIGURE 15. (*a*) Successful comparison between Rutherford-like model (using fitting empirically the 'Rutherford parameters') and experimental results in TCV of the time evolution of an NTM width (from Kong *et al.* 2022). (*b*) 'Rutherford plot' (island width w as x-coordinateand time derivative of the island width $\mathrm{d}w/\mathrm{d}t$ as y-coordinate) for a nonlinear evolution of $m = 1$ tearing mode with $\Delta' = 2.5$ given by simulations of (3.1) and (3.2). In blue, the Rutherford behaviour of w_{sep} is plotted and compared with the Rutherford behaviour of w_1 in orange and the first Rutherford model (4.2) in green.

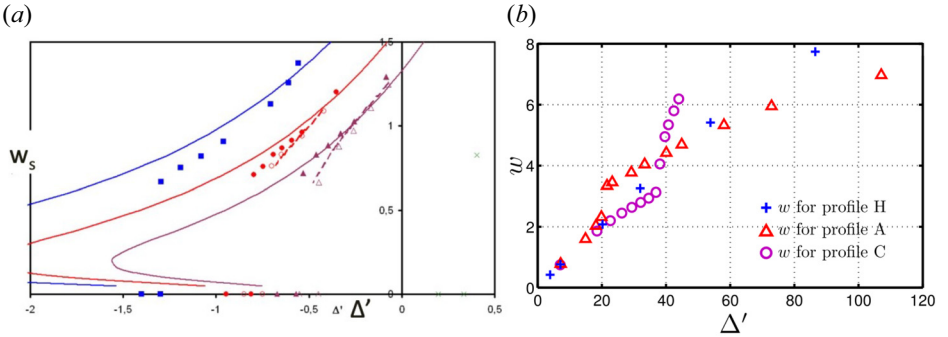

FIGURE 16. (*a*) Tearing mode magnetic island saturated width as a function of Δ' for three different magnetic equilibria (profile H, profile A and profile C)(reproduced from Poyé *et al.* (2013), with permission from AIP Publishing). (*b*) Agreement between Rutherford-like model and reduced-MHD simulations including bootstrap current for the saturated width prediction in the case of a metastable magnetic island having a small saturated width (reproduced from Militello *et al.* (2008), with permission from AIP Publishing).

equilibrium ψ_0 and the mode $m = 1$. Thus, projecting this nonlinear interaction on Ohm's law given by (3.1) for the $m = 1$ mode, one obtains the first Rutherford-like model given the nonlinear evolution of the $m = 1$ island width, i.e. w_1^{Ruth}:

$$\partial_t w_1^{\mathrm{Ruth}} = 1.22\eta\Delta'. \tag{4.2}$$

The comparison between the time evolution of w_{sep} and of w_1 (computed from simulations) to the first Rutherford model (4.2) is rich in teaching: in figure 15(*a*), a

https://doi.org/10.1017/S0022377824001363 Published online by Cambridge University Press

'Rutherford plot' is presented (i.e. plot having island width as x-coordinate and the time derivative of the island width as y-coordinate) for a nonlinear evolution of $m = 1$ tearing mode with $\Delta' = 2.5$ given by simulations of (3.1) and (3.2). In blue, the Rutherford behaviour of w_{sep} is plotted and compared with the Rutherford behaviour of w_1 in orange. One can conclude that the definition of the island width from the computation of separatrix positions w_{sep} is not equivalent to the definition given by Biskamp with (4.1). Indeed, in Biskamp's definition, only the $m = 1$ mode is taken into account whereas in nonlinear simulation, the resulting magnetic island observed on the contour plot of ψ results from nonlinear interactions of all the simulation modes. It then comes that, naturally, the evaluation of the island width from Biskamp's definition is underestimated since only one mode is taken into account. Then, the first model of Rutherford (4.2) is also plotted in green in figure 15(a). This first model gives the maximum growth of the $m = 1$ tearing mode, but fails at predicting the saturation width. The model has to be improved.

4.1.2. *Discussion on the improved Rutherford-like models*

These improvements were not long in coming. From the Rutherford behaviour of the $m = 1$ mode (orange line in figure 15a), one can decompose the dynamics of a tearing island into two phases. The first linear phase is called the 'Rutherford regime'. Then, once the island growth reaches its maximum given by (4.2), the system enters into the second phase which is fully nonlinear and called the 'exponential regime' since the island growth decays exponentially. Escande & Ottaviani (2004) and Militello & Porcelli (2004), with the well-known 'POEM' model, improved the pioneering work of Rutherford with (4.2) by catching this exponential phase and by giving a physical picture to the saturation of the $m = 1$ tearing mode for the time. The method is equivalent to that used by Rutherford to derive (4.2). Indeed, the POEM model is derived by projecting Ohm's law (3.1) on the $m = 1$ mode at the resonance following Biskamp's definition of the island width (and using $\psi_1(x = \text{res})$). However, this model takes into account for the first time the important role played by the flow (i.e. ϕ) by keeping the magnetic flux advection term in Ohm's law. The saturation mechanism of the tearing mode can be understood only by considering the energy transfer between the island and the flow. As a consequence, one can conclude that the coupling between the island and the flow participates first to the drive of the island growth (in the linear phase with the characteristic quadrupole structure observed on ϕ in figure 6a). Then, once the magnetic energy has been transferred through kinetic energy to the flow, the island growth decreases until the island reaches its saturated width which can be predicted by the POEM model:

$$\partial_t w_1 = 1.22\eta\Delta' - 1.22\eta\frac{0.41}{a^2}w_1. \tag{4.3}$$

Although this model gives for the first time an elegant physical picture of the role played by the flow in the tearing physics (in linear phase as well as in nonlinear phase), the hypothesis of the calculation (evaluation of only the mode $m = 1$, evaluation at the resonant surface only, 'ψ-constant' approximation and small Δ' regime) limit strongly the validity of the model (Poyé *et al.* 2014; Muraglia *et al.* 2021). Moreover, the Rutherford behaviour of an $m = 1$ island predicted by the POEM model (4.3) (purple line in figure 17b Muraglia *et al.* 2021) is a line describing the exponential growth that does not follow the island dynamics computed from simulations taking into account evolution of $m = 0$ and $m = 1$ modes (green dashed line in figure 17a).

Later, Smolyakov *et al.* (2013) improved the model again by taking into account the perturbation of the equilibrium due to the magnetic island growth i.e. by taking into account the nonlinear interaction between $m = 0$ and $m = 1$ modes. This model is known

https://doi.org/10.1017/S0022377824001363 Published online by Cambridge University Press

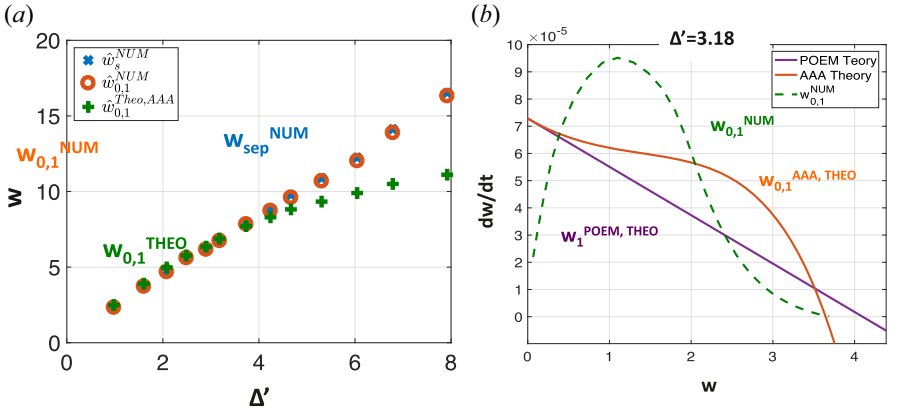

FIGURE 17. From Muraglia *et al.* (2021). (*a*) Rutherford diagram for a tearing mode, comparison of Rutherford-like models (POEM model and AAA model) with the island dynamic obtained from simulations taking into account evolution of $m = 0$ and $m = 1$ modes. (*b*) Comparison of the AAA model with numerical results for the prediction of the saturated width as a function of Δ'.

as the 'Smolyakov' model ('AAA' model in the figures) and gives the island width evolution taking into account the two modes ($m = 0$ and $m = 1$) at the resonance:

$$\begin{aligned}\partial_t w_{0,1} = \alpha &\left(1 + \frac{0.0235 * w_{0,1}^2}{a^2}\right)^{3/2} \\ &- \beta \frac{w_{0,1}}{a^2} \frac{1 + (\delta + 0.0235)\, w_{0,1}^2/a^2}{1 - (\gamma - 0.0235)\, w_{0,1}^2/a^2} \\ &\times \left(1 + \frac{0.0235 * w_{0,1}^2}{a^2}\right), \end{aligned} \tag{4.4}$$

where $\alpha = 1.22\eta\Delta'$, $b = \psi_0''(0)/\psi_0^{IV}(0)$,$\beta = 1.22\eta\frac{1.828}{\pi\sqrt{2}}$, $\delta = -0.0485 - 0.0732 * k_m^2 a^2 - 0.00201 * a^4/b^4$ and $\gamma = 0.6710/8\pi$. To test the validity of this model by comparing with numerical results, Biskamp's definition (4.1) cannot be used any longer since the mode $m = 0$ is not taken into account. However, following Biskamp, one can define a new definition of island width for the coupling between $m = 0$ and $m = 1$:

$$w_{1,0} = 4\sqrt{2\tilde{a}\left(\psi_1^{\text{res}}\right)}, \tag{4.5}$$

where $\tilde{a}$ is the magnetic shear at saturation. Figure 17(*a*) (from Muraglia *et al.* 2021) evaluates the ability of the AAA model (4.4) to predict the saturated island width as a function of Δ'. The green crosses give the predictions from the AAA model (4.4) and have to be compared with the orange circles that give the width prediction from numerical simulations and using (4.5) as definition. The AAA model improves the prediction (compared with the POEM model) to medium value of Δ', but fails to give a good prediction for large Δ' values, i.e. large islands. Moreover, figure 17(*b*) shows that as for the POEM model, the AAA model cannot predict the dynamic island (by comparing the numerical dynamics in green and the dynamics given by the model (4.4) in orange).

https://doi.org/10.1017/S0022377824001363 Published online by Cambridge University Press

An important feature comes from figure 17(*a*): a good agreement (even for the large Δ' regime) is found between the saturated width computed numerically from the separatrice's position (w_{sep} in blue in the figure) and the width computed numerically with a definition taking into account the nonlinear interaction between $m = 0$ and $m = 1$ modes. This implies that taking into account higher modes (as $m = 2$ mode) in a new Rutherford-like model will not improve the prediction. The discrepancy between models and simulations is coming from other missing element(s) in the theory and currently, new method(s) have to investigate how to improve the tearing mode saturation prediction. In particular, Loizu *et al.* (2020) investigated tearing mode saturation through the energy principle (Strauss 1976; Biskamp 2000). Moreover, from Militello *et al.* (2014); Poyé *et al.* (2013), some insights on the missing physics can be found. Indeed, the models presented, (4.2), (4.3) and (4.4), have been compared (in figure 17) to simulation results using a Biskamp-like definition for the island width, (4.2) and (4.5), where only the contribution of the resonant surface to the perturbation of ψ is taken into account. This strong assumption leads to the 0-D characteristic of Rutherford-like models where linear (growth rate) and nonlinear (saturated width) dynamics can be deduced from only one scalar parameter Δ'. However, Poyé *et al.* (2013) and Militello *et al.* (2014) showed that for two different magnetic equilibria having the same Δ' value, the resulting island dynamics is different. In particular, in figure 16(*b*) taken from Poyé *et al.* (2013), it is clearly shown that three different magnetic equilibria having the same Δ' lead to three different saturation widths. From this strong result, one can conclude that to improve the Rutherford-like model, one can take into account the global feature of the magnetic equilibrium and not only the contribution of the resonant surface to the saturation. This work is actually in progress.

4.2. *About the predictability of the saturated width of neoclassical tearing mode(s) in modern fusion devices*

4.2.1. *Prediction of NTM dynamics and saturation with generalized Rutherford model*

In fusion devices, the tearing mode is usually stable. However, bootstrap current can amplify a seed magnetic island and lead to the nonlinear growth of an NTM that can have dramatic consequences for the discharge and the device itself. As a consequence, the NTM predictability in terms of behaviour and saturation are of utmost importance for successful fusion by magnetic confinement. In that context, Rutherford-like models including bootstrap effects have been widely and successfully used in experiments to control and reduce NTM (La Haye 2006; Sauter *et al.* 2010; Kong *et al.* 2020, 2022). NTM leads to a current deficit in the island, and control strategies consist in compensating for this deficit by depositing a highly localized power inside the island. More precisely, to reduce and even suppress the island, electron cyclotron resonant heating and electron cyclotron current drive are used to inject the required current. These techniques, which have met with great success in various tokamaks, are based on the NTM dynamics predictions from Rutherford-like model(s) including bootstrap current (Carrera *et al.* 1986; Sauter *et al.* 1997):

$$\partial_t w_1 = 1.22\eta\Delta' - 1.22\eta\frac{0.41}{a^2}w_1 + \alpha C_b v^\star \frac{w_1}{w_1^2 + w_d^2}. \tag{4.6}$$

Here, w_d is deduced from the critical island width w_c (3.17) from which pressure flattening starts, i.e. $w_d = 1.8w_c$ (Fitzpatrick 1995; Militello *et al.* 2008; Agullo *et al.* 2014). The parameter α should be equal to one and is added to fit the model to experimental or numerical data. In figure 15(*a*) taken from Kong *et al.* (2022), a successful comparison (by empirical fitting) between Rutherford-like model and experimental NTM width

https://doi.org/10.1017/S0022377824001363 Published online by Cambridge University Press

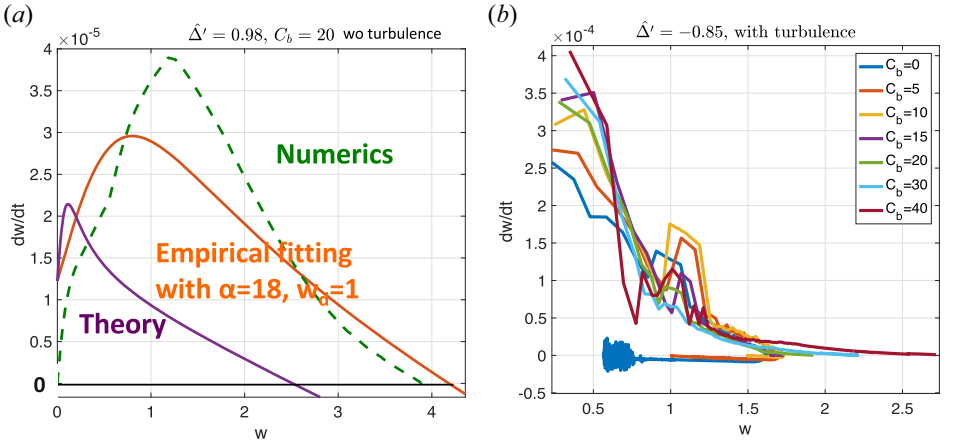

FIGURE 18. From Muraglia *et al.* (2021). (*a*) Impact of the seeding mechanism on the NTM dynamics. (*b*) NTM without turbulence and seeding by unstable tearing mode ($\Delta' = 0.98$), width evolution from numerical simulations of (3.14), (3.15), (3.16) in green, from empirical fitting of (4.6) and from (4.6) computing the exact value of w_d and taking $\alpha = 1$.

evolution in TCV is presented. This is typically what is used to control NTM width in fusion devices. However, as expected by theoretical results on the tearing mode saturation prediction, the comparison of the Rutherford-like model including bootstrap current (4.6) and numerical simulations without fitting any parameters fails. Figure 18(*a*) taken from Muraglia *et al.* (2021) shows disagreement between the evolution of w_1 from the model (4.6) with $\alpha = 1$, and computing the exact value of w_d (in purple) and the evolution of w_1 from nonlinear simulations of NTM using (3.14), (3.15) and (3.16) (with the dashed green line). The discrepancy can be reduced with the condition of fitting α and w_d: the empirical fitting with $\alpha = 18$ and $w_d = 1$ (in orange) shows a relatively good agreement with the numerical results (in green). One can note that the systematic comparisons between theoretical models and simulations (Muraglia *et al.* 2021) do not take into account the polarization current. However, in a recent work (Dudkovskaia *et al.* 2023), it has been shown that this current impacts the NTM threshold. In future work, it could be very interesting to investigate also its impact on NTM saturation.

4.2.2. *Impact of seed island mechanism on NTM dynamics and saturation*

The Rutherford-like model including bootstrap effects (4.6) is a 0-D model taking into account for the seeding mechanism only the Δ' parameter suggesting that the nonlinear evolution of the NTM does not depend on the physical nature of the seed. In figure 18(*a*) taken from Muraglia *et al.* (2021), the NTM has been seeded by an unstable tearing mode with $\Delta' = 0.98$. However, in figure 18(*b*), numerical simulations are shown for NTM having $\Delta' < 0$ and seeding by turbulence. The two evolutions suggest that the seeding mechanism impacts the nonlinear evolution of the NTM and its saturated width. One can conclude that future improved Rutherford-like model(s) taking into account bootstrap current have to take into account also the seeding mechanism. One can also note that the threshold mechanism of the bootstrap current is well recovered for NTM seeding by turbulence: figure 18(*b*) shows that for weak bootstrap current (i.e. weak C_b), the TDMI is not amplified to an NTM. Here, C_b has to be strong enough to drive NTM from TDMI as in the absence of turbulence.

https://doi.org/10.1017/S0022377824001363 Published online by Cambridge University Press

5. Conclusion

Here, based on a review of past works, a new paradigm to understand the multi-scale physics of a magnetic island in hot magnetized plasmas is proposed. The dynamics of magnetic island can be decomposed into three different steps which are called here the the magnetic island life steps.

First, the magnetic reconnection process at the origin of a magnetic island is the result of a non-ideal phenomenon that breaks the frozen-in law by not conserving the magnetic connectivity. Considering a slab configuration with a strong guide field going in the direction labelled as the parallel direction, any physical phenomenon that leads to the generation of a parallel electric field is at the origin of magnetic reconnection and of magnetic island structure(s). In hot magnetized plasmas of a fusion device, resistivity (i.e. collisions) and electronic inertia can originate at non-ideal small-scale magnetic reconnection processes.

In the future, the relevance for a fusion device of other non-ideal mechanisms leading to magnetic reconnection has to be explored. In particular, the question of the kinetic effect(s) or small-scale turbulence as possible sources of a parallel electric field has to be addressed.

Second, the resulting magnetic island structure(s) has to be driven. Here, it has been shown that a rich variety of possible mechanisms exists that drive the growth of a magnetic island. The so-called resistive large-scale tearing mode is usually stable in a fusion device. In general, the island(s) observed are neoclassical tearing mode(s) and result(s) from the amplification of a seed island by bootstrap current. In theory and simulations (using MHD as well as gyrokinetic frameworks), it also has been found that turbulence at small scale can drive a large-scale magnetic island in the presence or not of collisions. These turbulence driven magnetic islands (TDMIs) can be amplified by bootstrap current. At small scale, in simulations of the JET-ILW pedestal, electron temperature gradient can drive microtearing modes in the situation where the equilibrium magnetic field is stable from the tearing point of view stability. The linear growth of the MTM is amplified by the presence of the electric potential and the magnetic drift.

The novelty of this approach is to consider that the origin of magnetic reconnection (step one) and the drive of the resulting magnetic island structure(s) (step two) are not led by the same physical mechanism. This new approach allows to define a new characteristic reconnection time $\tau_{RM} \sim \sqrt{\tau^{I}_{\mathrm{Origin}} \tau^{L}_{\mathrm{Drive}}}$ that reflects the multi-scale and multi-physics aspects of magnetic reconnection process. This new definition of the reconnection time has to be checked by simulations investigating different mechanisms that drive the island. This is an ongoing work that will deserve future publication. Moreover, future works will also investigate new relevant physical mechanisms driving large-scale or small-scale magnetic island(s) in fusion devices.

Third, the magnetic island reaches a saturated state. The prediction of the nonlinear behaviour and saturation of a large-scale magnetic island is of utmost importance in a fusion device to limit and control its impact on the discharge. Rutherford-like model(s) based on fits with experimental data have been used successfully in various fusion devices to reduce and even suppress NTM. However, a lack of fundamental understanding of the saturation mechanism persists, and systematic comparisons between models and nonlinear MHD simulations(s) have failed.

In future works, the global radial of the magnetic equilibrium has to be taken into account in new improved Rutherford-like model(s) predicting tearing mode saturated width. Moreover, the origin of the NTM seeding mechanism has to be added in Rutherford-like models including bootstrap current effects. At small scale, the saturation

https://doi.org/10.1017/S0022377824001363 Published online by Cambridge University Press

mechanism of the microtearing mode is a fully open question that should be investigated to evaluate the impact of an MTM in the electron heat transport in a tokamaks pedestal.

Finally, the impact of saturated TDMIs on transport is still an open question that needs to be investigated in future work in the context of disruptions as well as the context of ELMs.

Acknowledgements

The authors want to thank D. Borgogno, D. Grasso, M. Hamed, E. Poli, A. Poyé, M.J. Pueschel, D. Villa and F. Widmer for fruitful discussions.

Editor P. Helander thanks the referees for their advice in evaluating this article.

Funding

This work is supported by the Eurofusion Enabling Research 'T-RecS' Project (CfP-FSD-AWP24-ENR). Centre de Calcul Intensif d'Aix-Marseille is acknowledged for granting access to its high-performance computing resources.

Declaration of interests

The authors report no conflict of interest.

REFERENCES

AGULLO, O., MURAGLIA, M., BENKADDA, S., POYÉ, A., DUBUIT, N., GATBET, X. & SEN, A. 2017*a* Nonlinear dynamics of turbulence driven magnetic islands. I. Theoretical aspects. *Phys. Plasmas* **24**, 042308.

AGULLO, O., MURAGLIA, M., BENKADDA, S., POYÉ, A., DUBUIT, N., GATBET, X. & SEN, A. 2017*b* Nonlinear dynamics of turbulence driven magnetic islands. II. Numerical simulations. *Phys. Plasmas* **24**, 042309.

AGULLO, O., MURAGLIA, M., POYÉ, A., BENKADDA, S., YAGI, M., GARBET, X. & SEN, A. 2014 A signature for turbulence driven magnetic islands. *Phys. Plasmas* **21**, 092303.

ALFVÉN, H. 1950 *Cosmical electrodynamics*. Oxford University Press.

APPLEGATE, D.J., ROACH, C.M., CONNOR, J.W., COWLEY, S.C., DORLAND, W., HASTIE, R.J. & JOINER, N 2007 Micro-tearing modes in the mega ampere spherical tokamak. *Plasma Phys. Control. Fusion* **49**, 1113.

AXFORD, W.I. 1984 Magnetic field reconnection. *Geophys. Monograph Ser.* **30**, 1–8.

BARDÓCZI, L., CARTER, T.A., LA HAYE, R.J., RHODES, T.L. & MCKEE, G.R. 2017 Impact of neoclassical tearing mode–turbulence multi-scale interaction in global confinement degradation and magnetic island stability. *Phys. Plasmas* **24**, 122503.

BISKAMP, D. 2000 *Magnetic Reconnection in Plasmas*. Cambridge University Press.

CARRERA, R., HAZELTINE, R.D. & KOTSCHENREUTHER, M. 1986 Island bootstrap current modification of the nonlinear dynamics of the tearing mode. *Phys. Fluids* **29**, 899.

CASSAK, P.A., BAYLOR, R.N., FERMO, R.L., BEIDLER, M.T., SHAY, M.A., SWISDAK, M., DRAKE, J.F. & KARIMABADI, H. 2015 Fast magnetic reconnection due to anisotropic electron pressure. *Phys. Plasmas* **22**, 020705.

CHANG, Z., CALLEN, J.D., FREDRICKSON, E.D., BUDNY, R.V., HEGNA, C.C., MCGUIRE, K.M., ZARNSTORFF, M.C. & TFTR GROUP 1995 Observation of nonlinear neoclassical pressure–gradient–driven tearing modes in TFTR. *Phys. Rev. Lett.* **74**, 4663.

CHOI, M.J., BARDÖCZI, L., KWON, J.-M., HAHM, T.S., PARK, H.K., KIM, J., WOO, M., PARK, N.-H., YUN, G.S. & YOON, E. 2021 Effects of plasma turbulence on the nonlinear evolution of magnetic island in tokamak. *Nat. Commun.* **12**, 375.

COPPI, B., MARK, J.W.-K., SUGIYAMA, L. & BERTIN, G. 1979 Magnetic reconnection in collisionless plasmas. *Ann. Phys.* **119**, 370.

DICKINSON, D., ROACH, C.M., SAARELMA, S., SCANNELL, R., KIRK, A. & WILSON, H.R. 2013 Microtearing modes at the top of the pedestal. *Plasma Phys. Control. Fusion* **55**, 074006.

DOERK, H., JENKO, F., PUESCHEL, M.J. & HATCH, D.R. 2011 Gyrokinetic microtearing turbulence. *Phys. Rev. Lett*. **106**, 155003.

DRAKE, J.F. & LEE, Y.C. 1977 Kinetic theory of tearing instabilities. *Phys. Fluids* **20**, 1341.

DUBUIT, D., AGULLO, O., MURAGLIA, M., FRANK, J., GARBET, X. & MAGET, P. 2021 Dynamics of magnetic islands driven by ballooning turbulence. *Phys. Plasmas* **28**, 022308.

DUDKOVSKAIA, A.V., CONNOR, J.W., DICKINSON, D., HILL, P., IMADA, K., LEIGH, S. & WILSON, H.R. 2023 Drift kinetic theory of neoclassical tearing modes in tokamak plasmas: polarisation current and its effect on magnetic island threshold physics. *Nucl. Fusion* **63**, 126040.

DUNGEY, J.W. 1953 The motion of magnetic fields. *Mon. Not. R. Astron. Soc*. **113**, 679–682.

EBRAHIMI, F. & BHATTACHARJEE, A. 2023 Plasmoid-mediated reconnection during nonlinear peeling–ballooning edge-localized modes. *Nucl. Fusion* **63**, 126042.

ESCANDE, D.F. & OTTAVIANI, M. 2004 Simple and rigorous solution for the nonlinear tearing mode. *Phys. Rev.* A **323**, 278.

FITZPATRICK, R. 1995 Helical temperature perturbations associated with tearing modes in tokamak plasmas. *Phys. Plasmas* **2**, 825.

FRANK, J., AGULLO, O., MAGET, P., GARBET, X., DUBUIT, N. & MURAGLIA, M. 2020 A reduced MHD model for ITG-NTM interplay. *Phys. Plasmas* **27**, 022119.

FURTH, H.P., KILLEEN, J. & ROSENBLUTH, M.N. 1963 Finite-resistivity instabilities of a sheet pinch. *Phys. Fluids* **6**, 459.

FURTH, H.P., RUTHERFORD, P.H. & SELBERG, H. 1973 Tearing mode in the cylindrical tokamak. *Phys. Fluids* **16**, 1054.

GIOVANELLI, R.G. 1946 A theory of chromospheric flares. *Nature* **158**, 81–82.

GRANIER, C., TASSI, E., BORGOGNO, D. & GRASSO, D. 2021 Impact of electron temperature anisotropy on the collisionless tearing mode instability in the presence of a strong guide field. *Phys. Plasmas* **28**, 022112.

GRASSO, D., BORGOGNO, D., LOVEPREET, S. & SUBBA, F. 2022 Stability of a weakly collisional plasma with runaway electrons. *J. Phys. Conf. Ser*. **2397**, 012004.

GRASSO, D., BORGOGNO, D., TASSI, E. & PERONA, A. 2020 Asymmetry effects driving secondary instabilities in two-dimensional collisionless magnetic reconnection. *Phys. Plasmas* **27**, 012302.

GRASSO, D., TASSI, E. & WAELBROECK, F. 2010 Nonlinear gyrofluid simulations of collisionless reconnection. *Phys. Plasmas* **17**, 082312.

GUO, H.Y., BINDERBAUER, M.W., TAJIMA, T., MILROY, R.D., STEINHAUER, L.C., YANG, X., GARATE, E.G., GOTA, H., KOREPANOV, S. & NECAS, A. 2015 Achieving a long-lived high-beta plasma state by energetic beam injection. *Nat. Commun*. **6**, 6897.

HAMED, M., MURAGLIA, M., CAMENEN, Y. & GARBET, X. 2018*a* Stability of a slab collisional microtearing mode. *Contrib. Plasma Phys*. **58**, 529–533.

HAMED, M., MURAGLIA, M., CAMENEN, Y. & GARBET, X. 2018*b* A kinetic model for the stability of a collisional current sheet. *J. Phys. Conf. Ser*. **1125**, 012012.

HAMED, M., MURAGLIA, M., CAMENEN, Y., GARBET, X. & AGULLO, O. 2019 Impact of electric potential and magnetic drift on microtearing modes stability. *Phys. Plasma* **26**, 092506.

HAMED, M., PUESCHEL, M.J., CITRIN, J., MURAGLIA, M., GARBET, X. & CAMENEN, Y. 2023 On the impact of electric field fluctuations on microtearing turbulence. *Phys. Plasma* **30**, 042303.

HARRIS, E.G. 1962 On a plasma sheath separating regions of oppositely directed magnetic field. *Nuovo Cimento* **23**, 115.

HATCH, D.R., KOTSCHENREUTHER, M., MAHAJAN, S.M., PUESCHEL, M.J., MICHOSKI, C., MERLO, G., HASSAN, E., FIELD, A.R., FRASSINETTI, L. & GIROUD, C. 2021 Microtearing modes as the source of magnetic fluctuations in the JET pedestal. *Nucl. Fusion* **61**, 036015.

HATCH, D.R., KOTSCHENREUTHER, M., MAHAJAN, S., VALANJU, P., JENKO, F., TOLD, D., GÖRLER, T. & SAARELMA, S. 2016 Microtearing turbulence limiting the JET-ILW pedestal. *Nucl. Fusion* **56**, 104003.

HATCH, D.R., PUESCHEL, M.J., JENKO, F., NEVINS, W.M., TERRY, P.W. & DOERK, H. 2012 Origin of magnetic stochasticity and transport in plasma microturbulence. *Phys. Rev. Lett*. **108**, 235002.

HAZELTINE, R.D., DOBROTT, D. & WANG, T.S. 1975 Kinetic theory of tearing instability. *Phys. Fluids* **18**, 1778.

https://doi.org/10.1017/S0022377824001363 Published online by Cambridge University Press

HELANDER, P., GRASSO, D., HASTIE, R.J. & PERONA, A. 2007 Resistive stability of a plasma with runaway electrons. *Phys. Plasmas* **14**, 122102.

HENDER, T.C., BURATTI, P., CASSON, F.J., ALPER, B., BARANOV, YU.F., BARUZZO, M., CHALLIS, C.D., KOECHL, F., LAWSON, K.D. & MARCHETTO, C. 2016 The role of MHD in causing impurity peaking in JET hybrid plasmas. *Nucl. Fusion* **56**, 066002.

HORNIG, G. & RASTÄTTER, L. 1997 The role of helicity in the reconnection process. *Adv. Space Res.* **19**, 1789–1792.

HORNIG, G. & RASTÄTTER, L. 1998 The magnetic structure of $B \neq 0$ – reconnection. *Phys. Scr.* **T74**, 34–39.

HORNSBY, W., MIGLIANO, P., BUCHHOLZ, R., GROSSHAUSER, S., WEIKL, A., ZARZOSO, D., CASSON, F.J., POLI, E. & PEETERS, A.G. 2016 The non-linear evolution of the tearing mode in electromagnetic turbulence using gyrokinetic simulations. *Plasma Phys. Control. Fusion* **58**, 014028.

HORNSBY, W., MIGLIANO, P., BUCHHOLZ, R., KROENERT, L., WEIKL, A., PEETERS, A.G., ZARZOSO, D., POLI, E. & CASSON, F.J. 2015*a* The linear tearing instability in three dimensional, toroidal gyro-kinetic simulations. *Phys. Plasmas* **22**, 022118.

HORNSBY, W., MIGLIANO, P., BUCHHOLZ, R., ZARZOSO, D., CASSON, F.J., POLI, E. & PEETERS, A.G. 2015*b* On seed island generation and the non-linear self-consistent interaction of the tearing mode with electromagnetic gyro-kinetic turbulence. *Plasma Phys. Control. Fusion* **57**, 054018.

ISAYAMA, A., MATSUNAGA, G., HIRANO, Y. & JT-60 TEAM 2013 Onset and evolution of $m/n = 2/1$ neoclassical tearing modes in high-β_p mode discharges in JT-60 U. *Plasma Fusion Res.* **8**, 1402013.

ISHII, Y., AZUMI, M. & KISHIMOTO, Y. 2002 Structure-driven nonlinear instability of double tearing modes and the abrupt growth after long-time-scale evolution. *Phys. Rev. Lett.* **89**, 205002.

ISHIZAWA, A., KISHIMOTO, Y. & NAKAMURA, Y. 2019 Multi-scale interactions between turbulence and magnetic islands and parity mixture–a review. *Plasma Phys. Control. Fusion* **61**, 054006.

KONG, M., SAUTER, O., FELICI, F., HOGEWEIJ, G.M.D., MERLE, A., NOWAK, S. & THE TCV TEAM 2020 On the triggerless onset of 2/1 neoclassical tearing modes in TCV. *Nucl. Fusion* **60**, 026002.

KONG, M., FELICI, F., SAUTER, O., GALPERTI, C., VU, T., HAM, C.J., HENDER, T.C., MARASCHEK, M., REICH, M. & THE TCV TEAM 2022 Physics-based control of neoclassical tearing modes on TCV. *Plasma Phys. Control. Fusion* **64**, 044008.

LA HAYE, R.J. 2006 Neoclassical tearing modes and their control. *Phys. Plasmas* **13**, 05550.

LOIZU, J., HUANG, Y. -M., HUDSON, S.R., BAILLOD, A., KUMAR, A. & QU, Z.S. 2020 Direct prediction of nonlinear tearing mode saturation using a variational principle. *Phys. Plasmas* **27**, 070701.

MAEYAMA, S., WATANABE, T.-H. & ISHIZAWA, A. 2017 Suppression of ion-scale microtearing modes by electron-scale turbulence via cross-scale nonlinear interactions in tokamak plasmas. *Phys. Rev. Lett.* **119**, 195002.

MAGET, P., FÉVRIER, O., GARBET, X., LÜTJENS, H., LUCIANI, J.-F. & MARX, A. 2016 Extended magneto-hydro-dynamic model for neoclassical tearing mode computations. *Nucl. Fusion* **56**, 086004.

MILITELLO, F., GRASSO, D. & BORGOGNO, D. 2014 The deceiving Δ': on the equilibrium dependent dynamics of nonlinear magnetic islands. *Phys. Plasmas* **21**, 102514.

MILITELLO, F., OTTAVIANI, M. & PORCELLI, F. 2008 Neoclassical tearing mode saturation in periodic current sheets. *Phys. Plasmas* **15**, 042104.

MILITELLO, F. & PORCELLI, F. 2004 Simple analysis of the nonlinear saturation of the tearing mode. *Phys. Plasmas* **11**, L13.

MURAGLIA, M., AGULLO, O., BENKADDA, S., GARBET, X., BEYER, P. & SEN, A. 2009*a* Nonlinear dynamics of magnetic islands imbedded in small-scale turbulence. *Phys. Rev. Lett.* **103**, 145001.

MURAGLIA, M., AGULLO, O., BENKADDA, S., YAGI, M., GARBET, X. & SEN, A. 2011 Generation and amplification of magnetic islands by drift interchange turbulence. *Phys. Rev. Lett.* **107**, 095003.

MURAGLIA, M., AGULLO, O., POYÉ, A., BENKADDA, S., DUBUIT, N., GARBET, X. & SEN, A. 2017 Amplification of a turbulence driven seed magnetic island by bootstrap current. *Nucl. Fusion* **57**, 072010.

MURAGLIA, M., AGULLO, O., YAGI, M., BENKADDA, S., BEYER, P., GARBET, X., ITOH, S.-I., ITOH, K. & SEN, A. 2009*b* Effect of the curvature and the β parameter on the nonlinear dynamics of a drift tearing magnetic island. *Nucl. Fusion* **49**, 055016.

MURAGLIA, M., POYÉ, A., AGULLO, O., DUBUIT, N. & GARBET, X. 2021 Nonlinear dynamics of NTM seeding by turbulence. *Plasma Phys. Control. Fusion* **63**, 084005.

PARKER, E.N. 1957 Sweet's mechanism for merging magnetic fileds in conducting fluids. *J. Geophys. Res*. **62**, 509–520.

PORCELLI, F. 1991 Collisionless $m = 1$ tearing mode. *Phys. Rev. Lett*. **66**, 425.

PORCELLI, F., BORGOGNO, D., CALIFANO, F., GRASSO, D., OTTAVIANI, M. & PEGORARO, F. 2002 Recent advances in collisionless magnetic reconnection. *Plasma Phys. Control. Fusion* **44**, B389.

POYÉ, A., AGULLO, O., MURAGLIA, M., GARBET, X., BENKADDA, S., SEN, A. & DUBUIT, N. 2015 Generation of a magnetic island by edge turbulence in tokamak plasmas. *Phys. Plasmas* **22**, 030704.

POYÉ, A., AGULLO, O., SMOLYAKOV, A., BENKADDA, S. & GARBET, X. 2013 Dynamics of magnetic islands in large Δ' regimes. *Phys. Plasmas* **20**, 020702.

POYÉ, A., AGULLO, O., SMOLYAKOV, A., BENKADDA, S. & GARBET, X. 2014 Dynamics of magnetic islands in large Δ' regimes. *Phys. Plasmas* **21**, 020705.

PREDEBON, I. & SATTIN, F. 2013 On the linear stability of collisionless microtearing modes. *Phys. Plasmas* **20**, 040701.

PRIEST, E. & FORBES, T. 1998 *Magnetic Reconnection – MHD Theory and Applications*. Cambridge University Press.

PUESCHEL, M.J., TERRY, P.W., JENKO, F., HATCH, D.R., NEVINS, W.M., GÖRLER, T. & TOLD, D. 2013 Extreme heat fluxes in gyrokinetic simulations: a new critical beta. *Phys. Rev. Lett*. **110**, 155005.

RUTHERFORD, P.H. 1973 Nonlinear growth of the tearing mode. *Phys. Fluids* **16**, 1903.

SAMOYLOV, M.J., IGOCHINE, M.J., YU, M.J., ZOHM, M.J. & THE ASDEX UPGRADE TEAM 2022 Magnetic reconnection rate during sawtooth crashes in ASDEX Upgrade. *Nucl. Fusion* **62**, 074002.

SAMOYLOV, O., IGOCHINE, V., YU, Q., ZOHM, H. & THE ASDEX UPGRADE TEAM 1997 Beta limits in long-pulse tokamak discharges. *Phys. Plasmas* **24**, 1654.

SAUTER, O., LA HAYE, R.J., CHANG, Z., GATES, D.A., KAMADA, Y., ZOHM, H., BONDESON, A., BOUCHER, D., CALLEN, J.D., CHU, M.S., *et al.* 1997 On the requirements to control neoclassical tearing modes in burning plasmas. *Plasma Phys. Control. Fusion* **52**, 025002.

SCHINDLER, K. & HESSE, M. 1988 General magnetic reconnection, parallel electric fields, and helicity. *J. Geophys. Res*. **93**, 5547–5557.

SETO, H., XU, X.Q., DUDSON, B.D. & YAGI, M. 2024 Two-stage crash process in resistive drift ballooning mode driven ELM crash. *Phys. Plasmas* **31**, 032513.

SMOLYAKOV, A., POYÉ, A., AGULLO, O., BENKADDA, S. & GARBET, X. 2013 Higher order and asymmetry effects on saturation of magnetic islands. *Phys. Plasmas* **20**, 062506.

SNYDER, P.B., WILSON, H.R., FERRON, J.R., LAO, L.L., LEONARD, A.W., OSBORNE, T.H., TURNBULL, A.D., MOSSESSIAN, D., MURAKAMI, M., XU, X.Q., *et al.* 2002 Edge localized modes and the pedestal: a model based on coupled peeling–ballooning modes. *Phys. Plasma* **9**, 2037.

SONNERUP, B.U.Ö. 1984 Magnetic field reconnection at the magnetopause : an overview. *Geophys. Monograph. Ser*. **30**, 92–103.

STRAUSS, H.R. 1976 Nonlinear, three-dimensional magnetohydrodynamics of noncircular tokamaks. *Phys. Fluids* **19**, 134.

SWEET, P.A. 1958*a* The neutral point theory of solar flares. *IAU Symp*. **6**, 123–134.

SWEET, P.A. 1958*b* The production of high energy particles in solar flares. *Nuovo Cimento Suppl. Ser. X* **8**, 188–196.

TAKEDA, K., AGULLO, O., BENKADDA, S., SEN, A., BIAN, N. & GARBET, X. 2008 Nonlinear viscoresistive dynamics of the $m = 1$ tearing instability. *Phys. Plasmas* **15**, 022502.

TASSI, E., GRASSO, D., BORGOGNO, D., PASSOT, T. & SULEM, P.L. 2018 A reduced Landau-gyrofluid model for magnetic reconnection driven by electron inertia. *J. Plasma Phys*. **84**, 725840401.

VASYLIUNAS, V.M. 1975 Theoretical models of magnetic field line merging. *Rev. Geophys. Space Phys*. **77**, 6271–6274.

WESTERHOF, E., BLANK, H.J. & PRATT, J. 2016 New insights into the generalized Rutherford equation for nonlinear neoclassical tearing mode growth from 2D reduced MHD simulations. *Nucl. Fusion* **56**, 036016.

YU, Q. & GÜNTER, S. 2022 Fast magnetic reconnection and driven plasma rotation in reversed central magnetic shear configuration. *Nucl. Fusion* **62**, 126056.

https://doi.org/10.1017/S0022377824001363 Published online by Cambridge University Press